Behavior of Connection with Beam Bearing on Bottom Flange of Girder

By

Wey-Jen Lee

Thesis submitted to the Faculty of the
Virginia Polytechnic Institute and State University
in partial fulfillment of the requirements for the degree of

MASTER OF SCIENCE
In
Civil Engineering

APPROVED:

_____

W.S. Easterling, Chairman

_____ _____

T.M. Murray R.H. Plaut

September 2001
Blacksburg, Virginia

Keywords: Yield Line Theory, Beam-to-Girder Connection, Finite Element Study

BEHAVIOR OF CONNECTION WITH BEAM BEARING ON BOTTOM FLANGE OF GIRDER

ABSTRACT

An analytical investigation was conducted to study the behavior of a bottom flange bearing beam-to girder connection subjected to patch loading. This connection would be useful with deep deck (thickness greater than 3 in.) composite slabs as well as with commonly used deck where floor-to-floor height needs to be minimized. Five girder specimens were loaded until yielding during the initial phase of the research. The analysis section consists of the yield line theory and finite element study that were used to develop a model to predict the collapse loads of the girder sections. These results from the model were then compared to the experimental loads. A design procedure utilizing the proposed model and future work recommendations are then presented.

Acknowledgements

I would like to express my sincere appreciation to my committee chairman, Dr. Samuel Easterling, for his guidance and patience during the development of this thesis. I would also like to thank Dr. Thomas Murray and Dr. Raymond Plaut for their help and advice in this research. I would like to convey my deepest thanks to Angela Terry for the initial work on this research, particularly in the testing program and the yield line analysis.

I would like to thank the Material Response Group for allowing me to use their computer facilities for my analysis, in particular Dr. Scott Case. I would also like to thank Aixi Zhou and Youngjin Woo for their helpful insights, particularly in the ANSYS study. My heartfelt thanks also go to Tze Wei Choo for her unwaveringly faith in me to finish this thesis.

Finally, I would like to express my gratitude and thanks to my family back home in Malaysia for their constant encouragement and advice. This thesis would not have been possible without their love and support.

TABLE OF CONTENTS

LIST OF FIGURES

Figures Page

LIST OF TABLES

CHAPTER 1
INTRODUCTION AND LITERATURE REVIEW

1.1 SCOPE AND OBJECTIVES OF RESEARCH

This research project focuses on a new type of beam-to-girder connection developed at Virginia Polytechnic Institute and State University. The connection consists of the beam bearing directly on the bottom flange of the girder as illustrated in Fig. 1-1. A lateral stabilizing angle and erection bolts through the bottom flanges are required to complete this connection. The connection is useful with deep deck (more than 3 in.) composite slabs to offset the increase in the floor depth caused by the additional slab depth, as well as with commonly used deck (less than or equal to 3 in.) in which floor-to-floor height needs to be minimized. This connection would also be economical and easy to construct.

The experimental portion of this study was conducted and reported by Terry and Easterling (2000), in which five beam specimens were loaded on both sides of the bottom flange to failure. The second phase of the research to verify the adequacy of the bottom flange bearing connection analytically is reported herein.

The objective of this study is to develop a yield line equation that accurately predicts the failure load (yielding) of the bottom flange of the bearing girder for a variety of sections. The yield line equation results are then compared with experimental results. A design procedure is formulated, which provides the nominal load, given the material strength and geometry of the section.

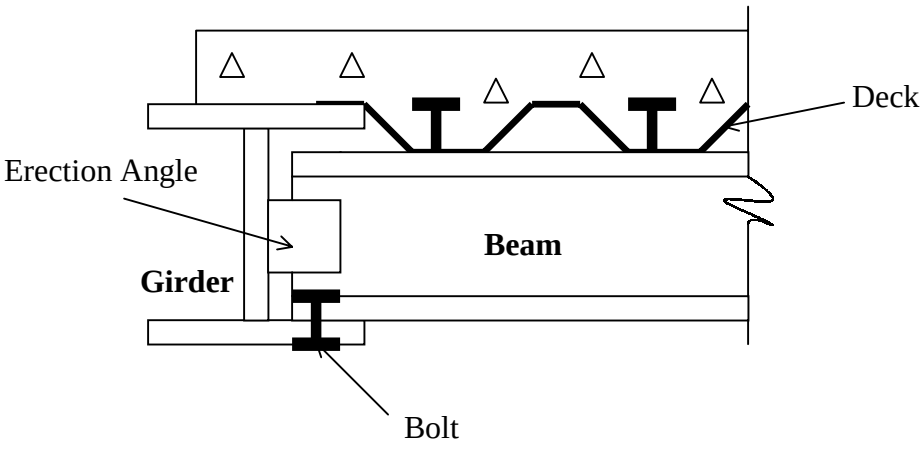

FIGURE 1-1. Proposed Beam-to-Girder Connection

1.2 METHODOLOGY

Structural analysis based on elastic theory generally gives a good approximation of a structure's deformations and stress-strain behavior in the service load range. However, it fails to determine the maximum load-carrying capacity of the structure in question, if inelastic behavior is prevalent. In addition, at impending failure, the basic assumptions of the elastic theory are no longer applicable. A suggested and simple method for analyzing the real load-carrying capacity of some structures is the yield line analysis.

The yield line analysis is an ultimate load method and is used more commonly in reinforced concrete slabs but can be applied to estimate the critical loads of steel plates, provided the pertinent ultimate moments are used and that the stress-strain behavior can be reasonably approximated by Johansen's rigid-plastic yield criterion (Szilard, 1974). The yield line analysis considers all possible failure mechanisms, which depend on the boundary and loading conditions of the plate. Then, the ultimate load of the structure would be the smallest failure load from those possible patterns. This critical load, given the correct yield pattern, is calculated by using either the Virtual Work or Equilibrium Methods. The disadvantage of these methods compared to other plastic analysis like the Hillerborg Strip method is that an assumed yield line pattern has to be chosen prior to any calculations.

It is must be noted that there are three necessary conditions for determining the collapse load of a structure, i.e., equilibrium, mechanism, and safety considerations. The method used in this study will be the kinematic (or mechanism) procedure. It assumes a mechanism (a particular yield line pattern) and it must satisfy equilibrium (external work is equal to the internal work done by the system). All this is considered assuming the structural system is safe, that is, the plastic moment is not exceeded anywhere in the structure.

Four main assumptions were used in the yield line analysis in this study:

1) The steel plate deforms plastically at failure and is divided into plate elements (constant thickness) by the yield line segments. Along these yield lines, the constant maximum moments are developed.
2) The behavior is assumed rigid-plastic. Therefore the elastic deformations within the plate elements are negligible compared with the plastic deformations about the yield line. Hence the plate elements remain plane after rotating physically at collapse condition.
3) The Virtual Work method is used in this analysis, i.e., work done due to the movement of the external loading is equal to the energy dissipated in the rotation of the yield lines. This method provides an upper-bound solution to the critical load.
4) The yield pattern that corresponds to the lowest failure load experiences only ultimate bending moments, i.e., there are no shear forces or twisting moments present along those yield lines. Further explanation is provided in the literature review section.

In this study, the Von Mises yield criterion is used to define the strength of the plate. It is applied here, since it usually fits the experimental data better compared to other theories and no prior knowledge of the relative magnitudes of the principal stresses is needed (Mendelson, 1968). The Von Mises stress, $\sigma_{vm,}$ is related to the principal stresses, σ_1, $\sigma_{2,}$ and $\sigma_{3,}$ through the relationship

$$\sigma_{vm}^2 = 0.5[(\sigma_1-\sigma_2)^2+(\sigma_2-\sigma_3)^2+(\sigma_3-\sigma_1)^2] \qquad (1.1)$$

Timoshenko and Woinowsky-Krieger (1959) state that for thin plates with large deflection compared to the plate thickness, membrane stresses are present if the plate edges are fixed and the deflection due to the applied load is sufficiently large. Therefore, the applied load now is transmitted partly by flexural rigidity of the plate and partly by membrane action. As the applied load is increased, so are the membrane forces and the plate will seem to have increased stiffness. However, for thin plates with small deflection compared to their thickness, membrane forces caused by the fixed edges in the plane of the plate are negligible. This is because the neutral axis in the steel does not move when load is applied, as it does in concrete behavior where arch action is developed (Gamble, 2001). In both cases, the actual behavior of the plate is strongly dependent on the restraint of axial deformations by the surrounding structure. For this study, the membrane action effects will be neglected.

Chapter Two describes the testing program that was reported by Terry and Easterling (2000) during the first phase of the research. Chapter Three presents the analytical study, which looks into the yield line theory and the finite element analysis. Chapter Four compares the experimental results with those of the analytical study. Chapter Five covers the design procedure utilizing the model developed from the yield line theory. The final chapter presents the conclusions and recommendations for future work on this research topic.

1.3 LITERATURE REVIEW

This chapter presents the literature review of the yield line theory as well as a brief general discussion of the theories involved in this area. Towards the latter part of the section, an overview of a study on structural tee hanger connections is presented, as it is similar to the beam-to-girder connection, i.e., vertical tensile forces are applied at the bottom flange on both sides.

Johansen (1962) first proposed the yield line theory, which is an upper bound approach for analyzing concrete slabs, in 1943. He identified several theorems related to the yield line analysis, including:

- The yield line between two parts of a slab must pass through the point of intersection of their axes of rotation. Deformations only occur in the yield lines consisting of relative rotation of the two adjoining parts of the slab about axes whose location depends upon the supports. The individual parts of the slabs are regarded as planes.
- The yield line pattern is determined by the axes of rotation of the various parts of the slab and the ratio between the rotations, i.e., if the slab is divided into n parts, and if all the axes of rotation are known, the yield pattern will depend only on the n-1 ratios between the rotations.
- The yield pattern corresponds to the maximum absolute value of the ultimate moment per unit length. To ensure that it is the right one, the individual parts of the slab must be investigated. If two yield patterns are possible, the yield lines from the pattern corresponding to the largest ultimate moment must divide up some of the parts of the slab of the other pattern.

In his second published work, Johansen (1972) considered a rectangular slab with uniformly distributed total load per unit length, and observed that it usually yields at the supports and along the span. He noted that the yield moment in a restrained slab is equal to the yield moment in a simply supported slab. By using equilibrium and work equations, he derived an equation for the above case:

$$\frac{pab}{8(1+\frac{b}{a}+\frac{a}{b})} \geq m \qquad (1.2)$$

where m is the moment, p is the total distributed load per unit length and a, b are slab dimensions that occur symmetrically, i.e., the formula is valid whether a > b or b > a.

According to Borgsmiller and Murray (1995), the yield line is a continuous formation of plastic hinges along a straight or curved line in a plate or slab structure. A failure mechanism is assumed to exist when the yield lines form a kinematically valid collapse mechanism. As a result, yield line theory is analogous to plastic design theory in which elastic deformations are negligible compared to the plastic deformations resulting from the yield lines. Even though much of the yield-line theory development is related to reinforced concrete slabs, the principles of this theory are applicable to steel plates.

It is suggested that the yield line mechanisms are best analyzed using the virtual work method, as it is more suitable for steel applications. In this method, external work done by the applied loads moving through a small arbitrary virtual deflection is set equal to the internal work done by the plate as it rotates along the yield lines to accommodate this virtual deflection, i.e., $W_e = W_{i.}$ The assumption is that a yield pattern has been formed, but the collapse load is merely imminent. As a result, the external forces and internal maximum moments are still in equilibrium. By setting the above equation, the relation between applied loads and the ultimate resisting moment is obtained. The resulting equation is solved for either the unknown failure load or unknown plate moment capacity.

Srouji et al. (1983) identified three guidelines in determining the location of a yield line in a steel plate:

- Axes of rotation generally lie along lines of support
- Yield lines pass through the intersection of the axes of rotation of adjacent plate segments
- Along a yield line, the bending moment is assumed to be a constant and equal to the plastic moment of the plate.

For the virtual work method, one first assumes a yield pattern, and therefore the axes of rotation and the ratios of the rotations are known. A set of simultaneous rotations is then used as the virtual displacements. Because all that is happening between the parts of a slab is rotation and not translation, the shear forces do not do any work in the slab as a

whole. Also, the work done by torsional moments is zero when summed over the entire slab, from the fact that work is equal and opposite on both sides of the yield line. Therefore, the internal work stored by an entire yield line mechanism is due only to bending moments and can be written as:

$$Wi = \sum_{n=1}^{N} m_p \theta_n L_n \tag{1.3}$$

where N is the number of yield lines in the mechanism, m_p is the plastic moment capacity of the plate, θ_n is the relative normal rotation of line n and work is stored in the n^{th} yield line of length $L_{n.}$ This is the case if m_p and θ_n are uniform along the length, $L_{n.}$ For complicated yield lines the expression above is resolved into x- and y- components, i.e.,

$$Wi = m_p \sum_{n=1}^{N} (\theta_{nx} L_{nx} + \theta_{ny} L_{ny}) \tag{1.4}$$

where θ_x and θ_y are components of θ_n in the x- and y- directions, respectively, and L_{nx} and L_{ny} are the projected lengths of the yield line in the x- and y- directions. Because the moment and rotation vectors are in the same direction, the internal work due to either positive or negative moments will always have the same signs. For steel plates:

$$m_p = \frac{F_{py} \; t_p^{\,2}}{4} \tag{1.5}$$

where F_{py} = yield stress of the plate material and t_p = plate thickness.

Each moment end-plate configuration has a different expression for internal work W_i due to unique yield line mechanisms. However, the external work, W_e, is the same for all end-plate configurations.

The external work due to a unit displacement at the outside of the beam tension flange, resulting in a rotation of the beam cross-section about the outside of the beam compression flange, is given by:

$$W_e = M_u\theta = M_u\,(1/h) \tag{1.6}$$

where M_u is the ultimate beam moment at the end plate and θ is the virtual rotation at the connection, equal to 1/h, where h is the total depth of the beam section.

Bakker (1990) presented the generalized yield line theory, which is an adaptation of the classical yield line method to analyze the load-deformation behavior of thin-walled steel members. The author pointed out that the upper bound limit analysis for nonlinear load deformation behavior and an appropriate yield criterion must be used. The membrane stresses will develop during the deformation of a thin-walled steel member and, thus, the Von Mises yield criterion should account for the influence of normal and in-plane shear forces. The author proposed that the full plastic moment of a steel plate should be

$$m_p = \frac{2}{\sqrt{3}} \frac{F_{py}\ t_p^{\,2}}{4} \tag{1.7}$$

since the previous expression is derived for fully plastic beams and is not valid for plates. This is because in a plate yield line, the strain rate tensor component vanishes, since the length of the yield line does not change and the normality condition applies.

The author also suggested the Exact Work method, which is basically the virtual work method for yield line analysis. This method includes in-plane normal and shear force deformations whereas the previous Virtual Work method presented by Srouji et al. (1983) only took into account rotational deformations in the yield lines caused by bending moments, i.e., $\Delta_n = \Delta_s = 0$. The Exact Work method equates the incremental energy dissipation in a yield line with the external incremental work being done.

The incremental energy dissipation discussed by Bakker (1990) is given below:

$$W_{\text{int}} = \int_0^L (m_b \Delta_b + n_n \Delta_n + n_s \Delta_s) \cdot dx \qquad (1.8)$$

where m_b, n_n, n_s are the bending moment, in-plane normal force and shear force per unit length of the yield line, respectively, with its corresponding incremental deformations. It is also noted that the Δ_n and Δ_s deformations influence the external incremental work because they are related to the incremental displacements of the rigid plate elements. Therefore, in the simplified virtual work method presented initially by Srouji et al. (1983), m_b will be reduced to m_p. The magnitude of n_n and n_s is determined from equilibrium conditions and not from incremental yield line deformations.

Theoretically, the yield line analysis is unsafe because it provides an upper bound solution, which is an over-estimate of the strength of the plate (Moy, 1996). However, in practice it is safe because the analysis ignores two important factors:

1) Moments of resistance of the plate are calculated ignoring strain hardening, which can significantly increase the strength of the steel plate. This reserve of strength is estimated to be about 10 percent of the calculated value.
2) Yield line theory is an idealization of slab behavior since it assumes bending action alone carries the vertical loads, although tests have shown that this is not the case. The load is in fact carried partly by bending as well as forces within the plane of the slab, called membrane action. The more the plate deflects, the more significant is the membrane action.

There are two types of membrane action. When the edges provide little or no restraint to horizontal movement (i.e., simply supported, for example), tensile membrane action occurs (Fig. 1-2). Since this type of edge does not provide horizontal restraint, both tensile and compressive stresses have to form in the plate to ensure horizontal equilibrium. The tensile stresses reduce the moment of resistance of the plate, whereas the compressive stresses increase the moment of resistance. In this case, the increase in

moment of resistance due to compressive force outweighs the reduction in moment of resistance due to tensile force, causing a load capacity increase in the plate up to 30 percent above the predicted results from the yield line theory. For edges that have horizontal restraint, compressive membrane action occurs. As the cracks open, the plate jams itself between the edges (Fig. 1-3). This jamming process will induce very large compressive stresses and may cause a load capacity increase of 200 percent or more above the yield line loads.

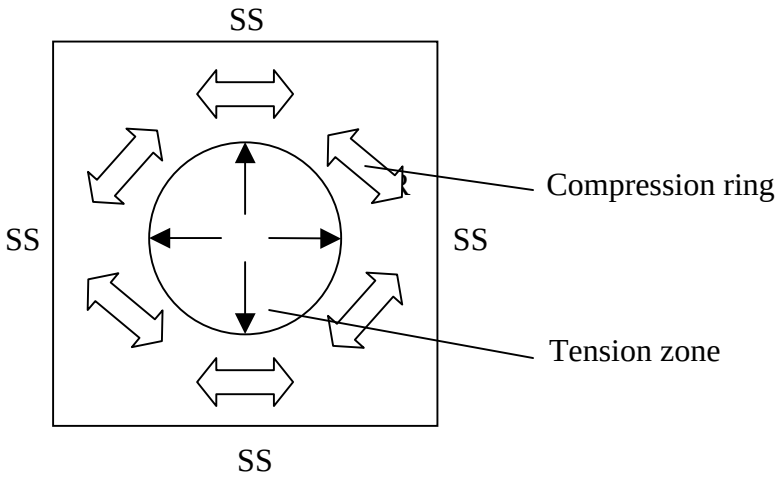

FIGURE 1-2. Tensile Membrane Action (Park and Gamble, 1980)

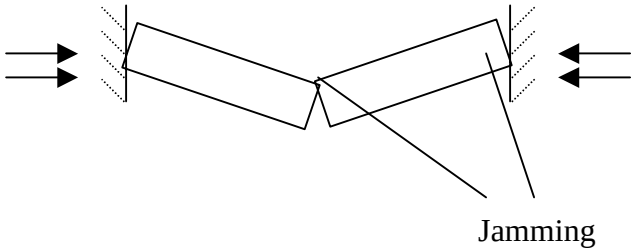

FIGURE 1-3. Compressive Membrane Action (Park and Gamble, 1980)

Park and Gamble (1980) looked extensively into yield line theory and membrane action for reinforced concrete slabs. Membrane forces are often present in reinforced concrete slabs (and steel plates) at the ultimate load as a result of boundary conditions and geometry of deformations. The yield line theory, which only considers the bending

moments at the yield lines, does not include these compressive or tensile membrane forces. The compressive membrane forces enhance the flexural strength (biaxial effect) of the slab sections at the yield lines, which will cause the slab's ultimate load to be greater than the ultimate load calculated using Johansen's yield line theory. The tensile membrane action is useful in preventing a catastrophic failure when the ultimate load is reached. However, membrane action is difficult to incorporate in the design process as a result of serviceability issues like excessive deflection or crack width.

Park and Gamble (1980) also presented an approximate relationship in determining the ultimate uniform load of a rectangular slab with three edges supported and one free end (Fig. 1-4), using the virtual work method. The authors assumed the corner yield lines are at 45° to the edges of the slab and looked into four different boundary conditions.

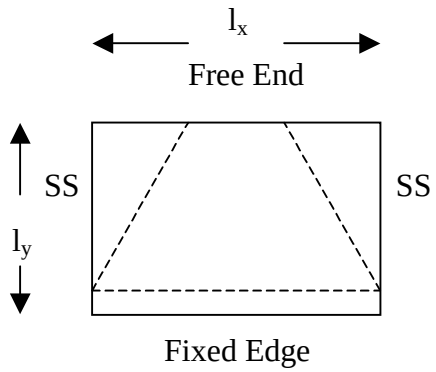

FIGURE 1-4. Yield Line Pattern for Fixed-end with Two-Simply Supported Edges (Park and Gamble, 1980)

The relationship for a fixed-end with two-simply- supported sides will be presented here:

$$w_u = \frac{6}{l_y{}^2[3(\frac{l_y}{l_x}) - 2]}[2(m_{ux} + m_{uy}) + \frac{l_x}{l_y} m'_{uy}] \qquad (1.9)$$

where w_u is the ultimate load, m_{ux} and m_{uy} are the bending moments in the x- and y-directions, respectively; m'_{uy} is the negative moment in the y-direction, and in steel it is

assumed that m'uy = m_{uy}. The relationship above is valid for l_x greater than or equal to 2 l_y.

Park and Gamble (1980) presented a comparison of the yield line theory ultimate load results with measured ultimate loads from tests conducted at the University of Illinois in 1956. This included the testing of five ¼-scale models of multi-panel reinforced concrete slabs, which were loaded until failure. Each of the floors contained nine 60-in. square panels arrayed three by three. Four of the floors were designed using the 1956 ACI Code while the other one was designed using a limit design method. Three specimens were flat slab floors while the other two were a beam-slab floor with stiff beams and a beam-slab floor with shallow beams, each 1 ½ - in. thick. For the beam-slab floor with stiff interior beams, a yield line analysis of the floor indicated a theoretical ultimate load of 467 psf whereas the measured ultimate load was actually 829 psf. This enhancement of the ultimate strength of panels (almost twice the theoretical yield line load) is due to the tensile membrane action, which is enforced by the lateral restraint of the surrounding beams. The latter beam specimen provided a similar result. The theoretical load was 388 psf while the measured ultimate load of the floor was 466 psf. This enhanced strength was caused by the increase in the flexural strength of the beam due to the compressive forces induced by tensile membrane action in the panels.

Jones and Wood (1967) discussed Johansen's yield analysis in detail as well as presented an extensive scope of the virtual work and equilibrium methods. They outlined the conditions that are required to establish an upper bound solution, which include:

- A valid mechanism of collapse which satisfies the boundary conditions must be found
- The internal dissipation of energy on the yield lines must equal the expenditure of energy due to external loads (virtual work equation)
- Either the material stays rigid or else deforms plastically
- Where deformation takes place, the direction of the strains is defined by the mechanism. The direction of the strains must, in turn, define the yield stresses required to calculate the dissipation of energy (yield criterion).

As mentioned before, since a structural tee hanger connection is similar to the connection being studied, a brief review of the work done on this subject is presented here. Otegui (1996) formulated a simplified method for determining the ultimate strength of structural tee hanger connections (Fig. 1-5), which is used to transfer tensile force to a support. The method covers two limit states: failure of the connection through plate yielding and through bolt rupture. The author used the yield line analysis to establish the yield capacity of the connection based on plate strength and a simplified Kennedy method for calculating the connection capacity based on bolt strength with prying action. The author then compared the predicted failure loads with fifteen connection tests results of both stiffened and unstiffened tee hangers. These specimens were fabricated from W8x18 beam sections and ½ -in. thick plates. Overall, both cases show conservative results, i.e., the ratio of the predicted failure load to the experimental failure load is less than one. However, for the thicker tee case, the result was unconservative. Finally, the author presented two design recommendations, depending on the limiting provisions of the design.

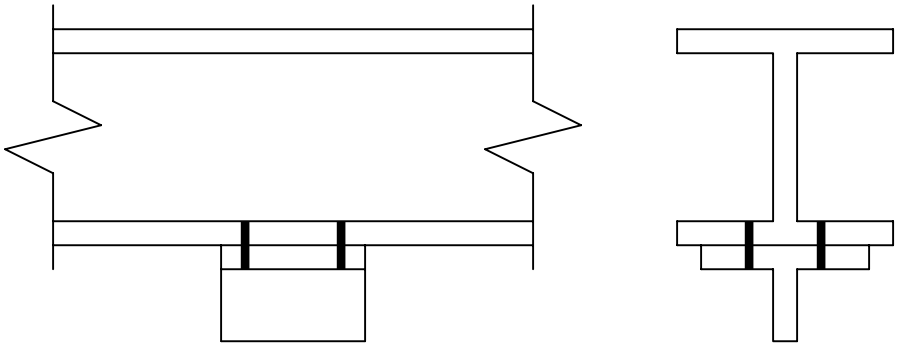

FIGURE 1-5. Tee Hanger Connection (Otegui, 1996)

Packer and Morris (1977) used the yield line theory to formulate a limit design method for a bolted beam-column connection. The authors looked at several failure mechanisms of a T-stub connected to a rigid base as well as column flanges undergoing lateral flexure. Rigid-plastic behavior was assumed for the yield lines, implying that strain hardening or membrane action is neglected. Failure is considered to occur when there are sufficient yield lines to form a mechanism. The end-plate thickness was found by equating the

plastic moment capacity to the applied moment and the bolt load was increased by 33 percent to account for prying action. The authors conducted a series of eight tests on T-stubs connected to columns representing the tension zone of an extended end-plate connection. Variables such as column flange thickness, bolt hole spacing, bolt preload and type of stiffening were studied with respect to the column flange behavior.

Mann and Morris (1978) also used the yield theory in their proposed limit design procedure of extended end-plate connections. Particular attention was given to the combined flexibility of the end-plate and column flange and its influence on overall joint behavior. However, the authors did not remove the bolt holes from the calculation of capacity. They claimed that the bolts contribute to the bending strength of the plates.

CHAPTER 2
TESTING PROGRAM

2.1 INTRODUCTION

The initial testing program of the research was reported by Terry and Easterling (2000). The objective of the testing program was to determine the actual yield line pattern development and ultimate load when the girder sections are being subjected to patch loads on the bottom flange that simulate the actual beam reaction. A test frame (Fig. 2-1) was fabricated to apply two equal vertical loads simultaneously on each side of the web, as would be the case for an interior girder. The girder was simply supported at both ends.

FIGURE 2-1. Test Set-up during the First Phase of the Research

2.2 TESTING PROCEDURES AND DETAILS

Before the test frame was put into place, each girder section was whitewashed in the center with a length of 3 ft to reveal the yield pattern that would take place during loading. Lateral braces were used at the top and bottom flanges of the test section approximately 1 ft 6 in. to either side of the loading point as shown in Figure 2-1. Load transmission was verified by placing redundant load cells at the test section supports and load point. Two loading options were used to transmit the load from the test frame onto the girder section. Option A (Fig. 2-2) transmits the load through a bearing plate on the girder bottom flange. Option B (Fig. 2-3) is more realistic in representing the load path of a beam-to-girder connection where the load is transmitted through a stub beam section with web stiffeners on the girder bottom flange. Displacement transducers and strain gages at multiple locations were used to record deflection and strain readings respectively, on the girder flange as load is being applied. Rosette strain gages were used because the direction of the principal stress was unknown prior to testing. The locations of the strain gages are illustrated and defined in Figure 2-4 and Table 2-1. Gages 1 and 2 were applied to the bottom surface of the test section's bottom flange. Gages 3 through 6 were applied to the top surface of the test section's bottom flange.

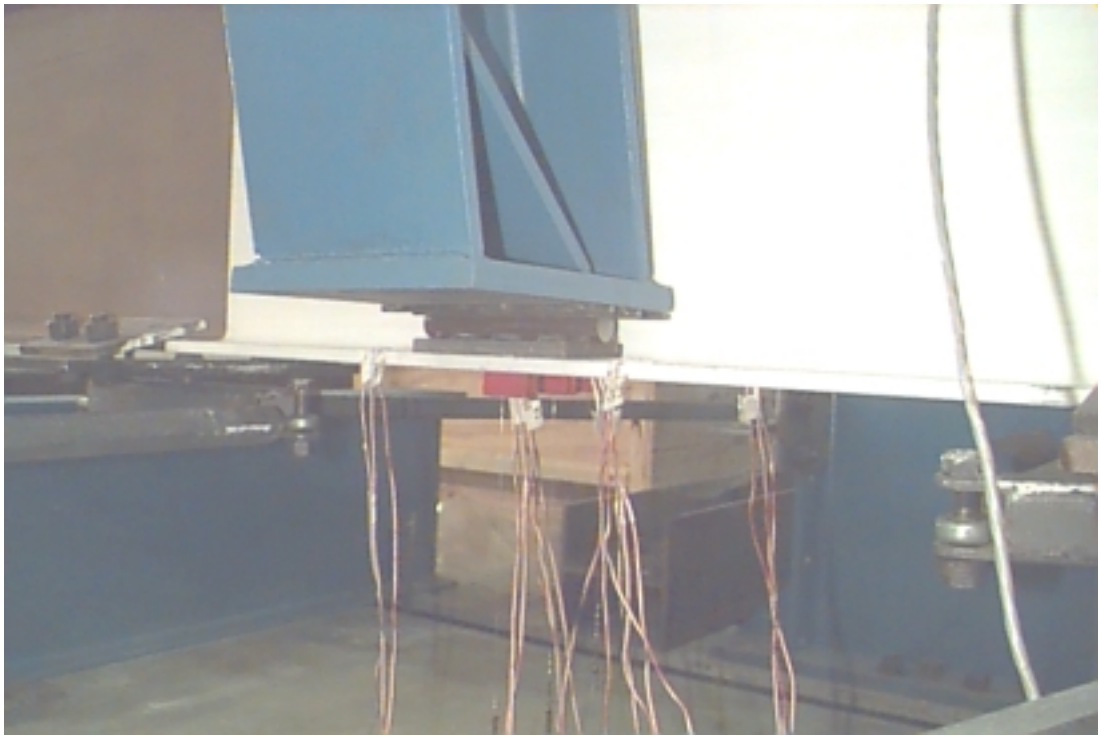

FIGURE 2-2. Loading Option A

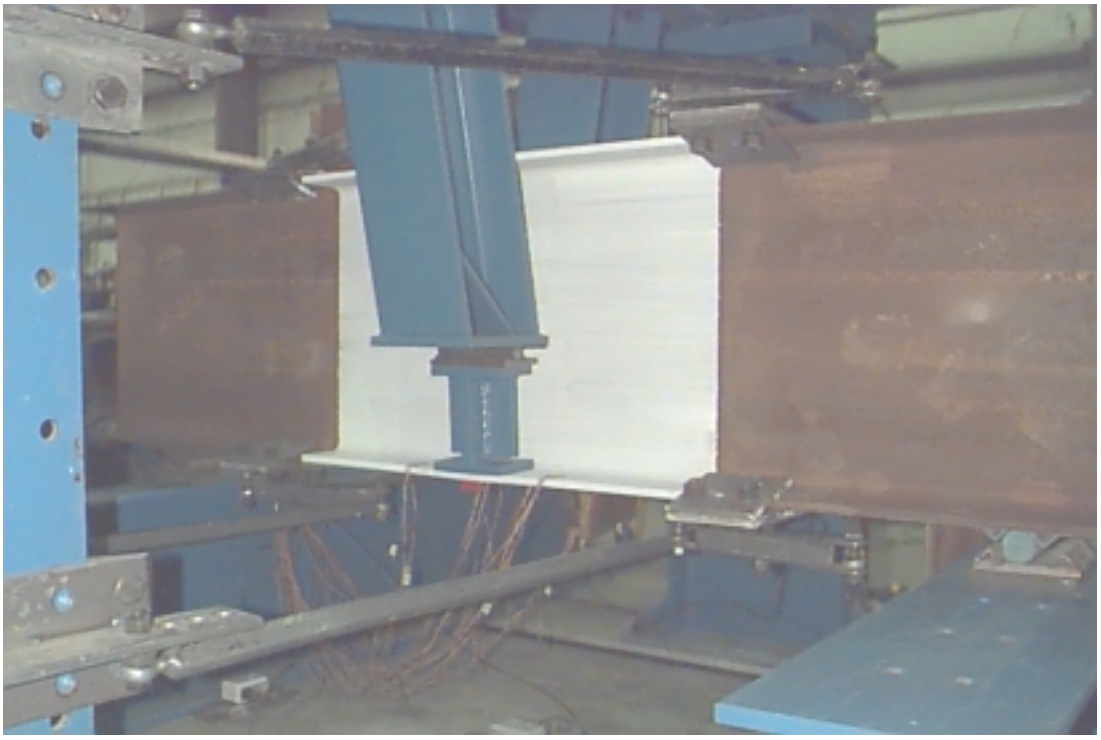

FIGURE 2-3. Loading Option B

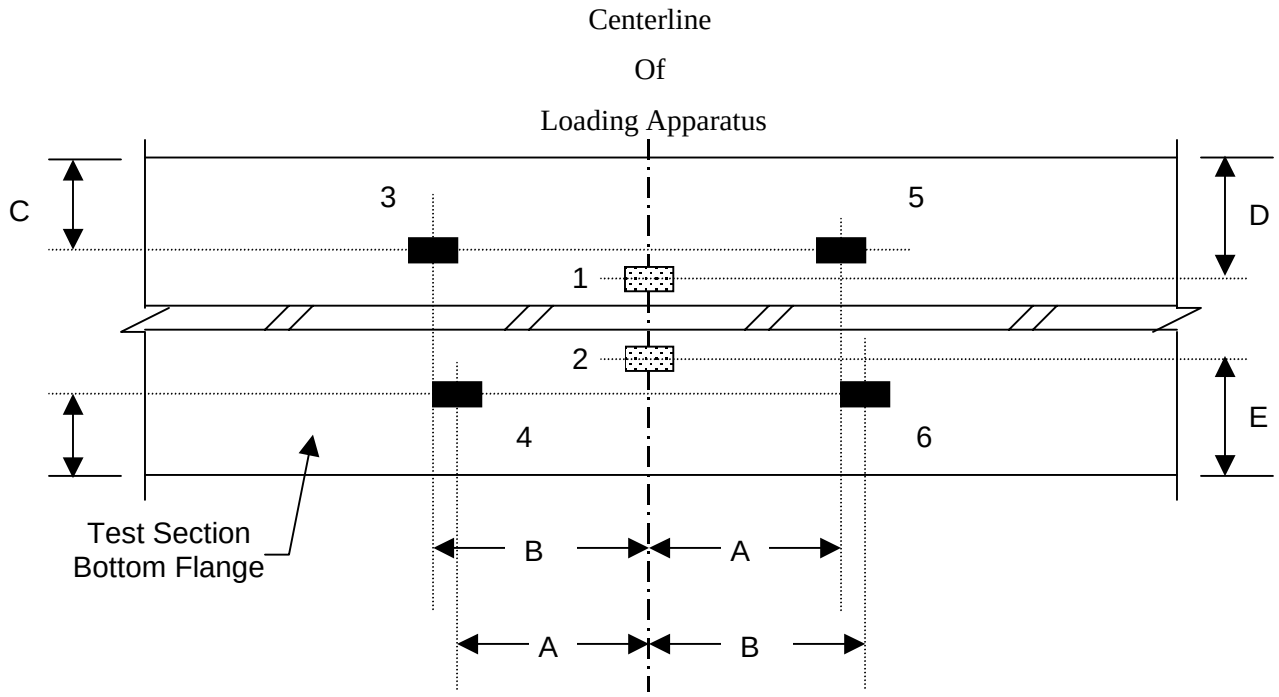

FIGURE 2-4. Strain Gage Locations on Girder Bottom Flange

TABLE 2-1. Strain Gage Locations on Girder Bottom Flange

Section	A (in.)	B (in.)	C (in.)	D (in.)	E (in.)
W21x44	4.50	5.50	1.75	2.25	2.25
W24x55	5.00	6.00	1.75	2.75	2.75
W18x40	4.50	5.75	1.50	2.25	2.25
W18x50	5.25	6.25	1.75	3.00	1.50
W24x68	6.00	7.00	2.00	3.75	1.50

2.3 GIRDER PROPERTIES

The five girder specimens were A572 Grade 50 steel (nominal 50 ksi yield stress). The actual yield and ultimate stresses of the five girder sections used in the testing program are obtained from the coupon tests. Those stress values and geometry properties of the girder sections are tabulated below (Table 2-2 and Table 2-3 respectively):

TABLE 2-2. Measured Yield and Ultimate Stresses for Girder Sections

Girder Section	F_y (ksi)	F_u (ksi)
W18x40	50.7	61.6
W18x50	54.9	69.5
W21x44	54.0	70.7
W24x55	58.4	75.3
W24x68	53.3	69.3

TABLE 2-3. Geometric Properties of Girder Sections

Girder Section	b_{fb} (in.)	b_{fg} (in.)	t_w (in.)	b_g (in.)	d (in.)	t_f (in.)
W18x40	6.5	6.02	0.32	2.85	17.90	0.53
W18x50	6.0	7.50	0.36	3.57	17.99	0.57
W21x44	6.0	6.50	0.35	3.08	20.66	0.45
W24x55	6.5	7.01	0.40	3.31	23.57	0.51
W24x68	6.5	8.97	0.42	4.28	23.73	0.59

where

b_{fb} = width of beam flange

b_{fg} = width of girder flange

t_w = thickness of girder web

$b_g = \frac{b_{fg}}{2} - k_1$

d = depth of girder

t_f = thickness of girder flange

2.4 EXPERIMENTAL RESULTS

The experimental results obtained from the testing program are tabulated in Table 2.4. The same yield pattern is observed in all five sections. Two out of the five girder spans were 6½ ft while the other three were 8 ft. To account for deflection due solely to the applied force at the mid-span, the relative deflection was obtained from the difference between the deflection at the edge of the flange and at the middle of the flange as illustrated in Figure 2-5. It can be seen that three out of the five girder sections experienced small relative deflections (less than the thickness of the flange) while the two largest sections had excessive relative deflections. Additional test results are presented in later sections as part of comparisons to analytical results.

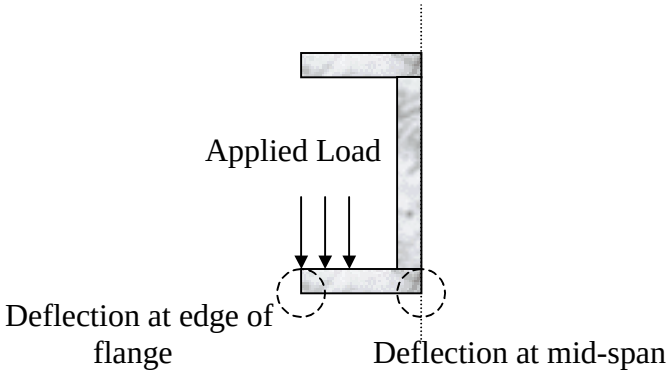

FIGURE 2-5. Cross Section of Girder at Mid-span

TABLE 2-4. Experimental Results (Terry and Easterling, 2000)

Girder Section	Fy (ksi)	Span (inch)	Load Application Method	Maximum Total Load (kips)	Maximum Relative Deflection (inch)
W21x44	54	96	Option A	79	0.32
W24x55	58	96	Option B	145	0.17
W18x40	51	96	Option B	169	0.20
W18x50	55	78	Option A	214	1.12
W24x68	53	78	Option B	280	0.79

CHAPTER 3
ANALYSIS STUDY

3.1 YIELD LINE ANALYSIS

The yield line analysis is used to develop the proposed yield line equation for the beam-to-girder connection. This equation predicts the load at first yield for common sections. The load at first yield is not the failure load of the girders but is considered the load value that would result in a flexural limit state in the absence of additional resistance. This additional resistance is mainly due to membrane action (Mays, 2000). The proposed yield line equation is derived in Appendix A. The predicted load values obtained from the equation are compared with the experimental and finite element results in Chapter Four. Using the Virtual Work Method and equating the external work applied with the internal work done, the following yield line equation is derived:

$$R_n = F_y t_f^2 \left[\frac{\frac{b_{fb}}{4b_g} + \frac{2}{\sqrt{2}}}{1 - \frac{N}{2b_g}} \right] \qquad (3.1)$$

where R_n = nominal strength of girder flange

F_y = yield strength of girder

t_f = thickness of girder flange

b_{fb} = width of beam flange

$b_g = \frac{b_{fg}}{2} - k_1$

N = length of beam bearing, i.e., $b_{fg} - ¾$ in.

The proposed equation relates the beam reaction R_n at yielding of the girder flange to the geometric and material properties of the beam and girder sections. Figure 3-1 shows the various geometric properties used in the proposed yield line equation. For constructability of the connection, a length of ¾ in. is used to determine the length of the beam bearing, N. The yield line equation corresponds to the yield line pattern as shown in Figure 3-2 (top pattern), which gives the lowest failure load. Several other yield line patterns were

also considered as depicted in Figure 3-2. In addition, observations of a similar yield line pattern (Fig. 3-3) for all the five girder sections during the testing program helped to determine the yield line pattern as well.

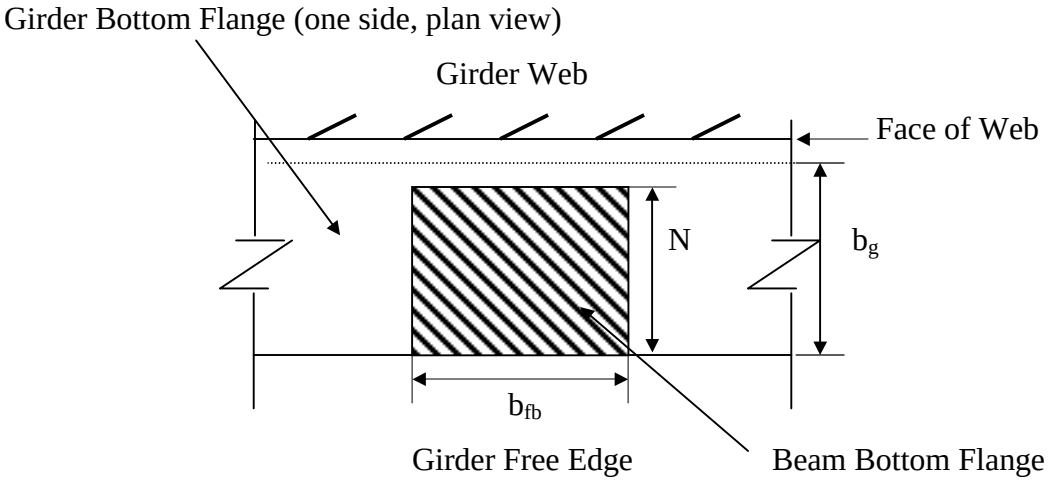

FIGURE 3-1. Section Properties Used in the Proposed Yield Line Equation

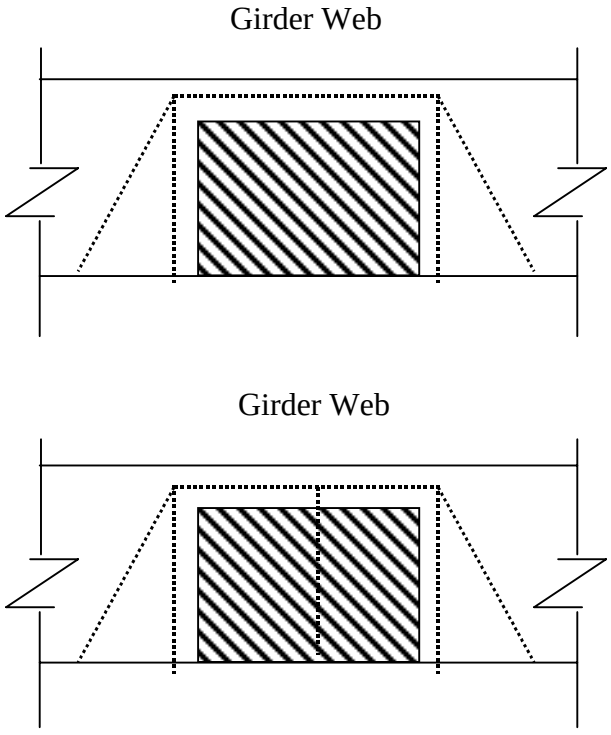

FIGURE 3-2. Samples of Yield Line Patterns

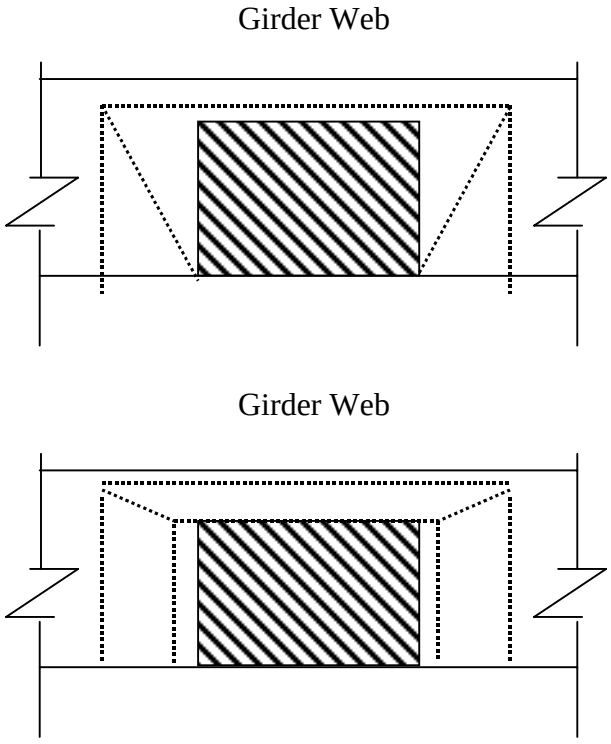

FIGURE 3-2. Samples of Yield Line Patterns (Continued)

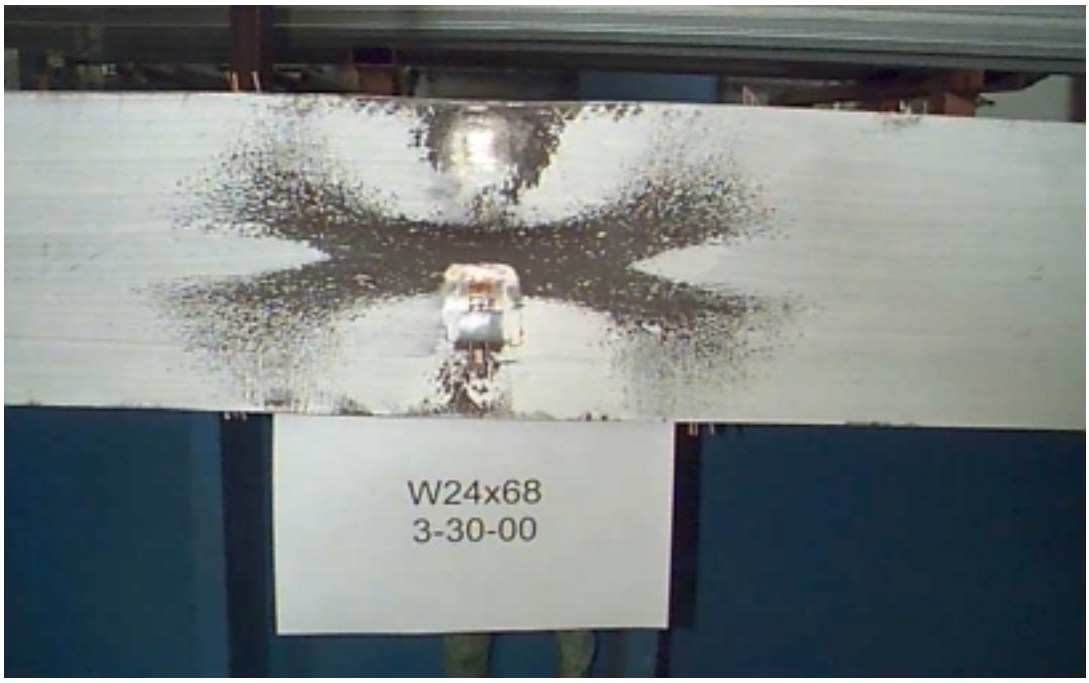

FIGURE 3-3. Yield Line Pattern Observed Throughout the Five Specimens (View of Bottom Flange from Below After Test)

3.2 FINITE ELEMENT STUDY

3.2.1 MATERIAL PROPERTIES

As a result of inconsistent data obtained in the testing program, a finite element study was conducted to validate the experimental results and perform additional "analytical" tests. The ANSYS software package was used to model the five girder sections, which were W18x40, W18x50, W21x44, W24x55 and W24x68. The SOLID45 (tetrahedral) element was used in the meshing process (Fig. 3-4). This element is defined with eight nodes with each having 3 degrees of freedom: translations in the nodal x-, y- and z-directions. The SOLID45 element was chosen mainly because it has plasticity, large deflection and strain capabilities. This will give an accurate representation of the actual spread of plasticity and yielding behavior of the girder model. The nonlinear stress-strain model that was chosen in this case is the Bilinear Kinematic Hardening (rate-independent plasticity) behavior, which uses a simplified bilinear stress-strain curve. This option assumes that the total stress range is equal to twice the yield stress. It is recommended for small strain use for materials that obey the Von Mises yield criterion, which includes steel. The yield stresses of the girder models are modeled according to the coupon test values while the tangent modulus is assumed to be 500 ksi. This tangent modulus was picked considering the actual stress-strain curve for steel, which is perfectly plastic after first yield, and some allowance to prevent the ANSYS solution from diverging (Fig. 3-5).

Elastic-plastic modeling of material stress-strain properties is used in this validation study. The accuracy of the finite element study is controlled by the mesh refinement. Therefore, coarse and fine meshes were considered for all five girder models. The mesh density is relative, i.e., the fine mesh is 30 percent more dense than the course mesh. For this study, the differences between the coarse mesh and fine mesh results were negligible and the coarse mesh was considered sufficiently accurate to reflect the actual girder behavior. Furthermore, the stress and strain results are validated with the corresponding theoretical values in Chapter Four.

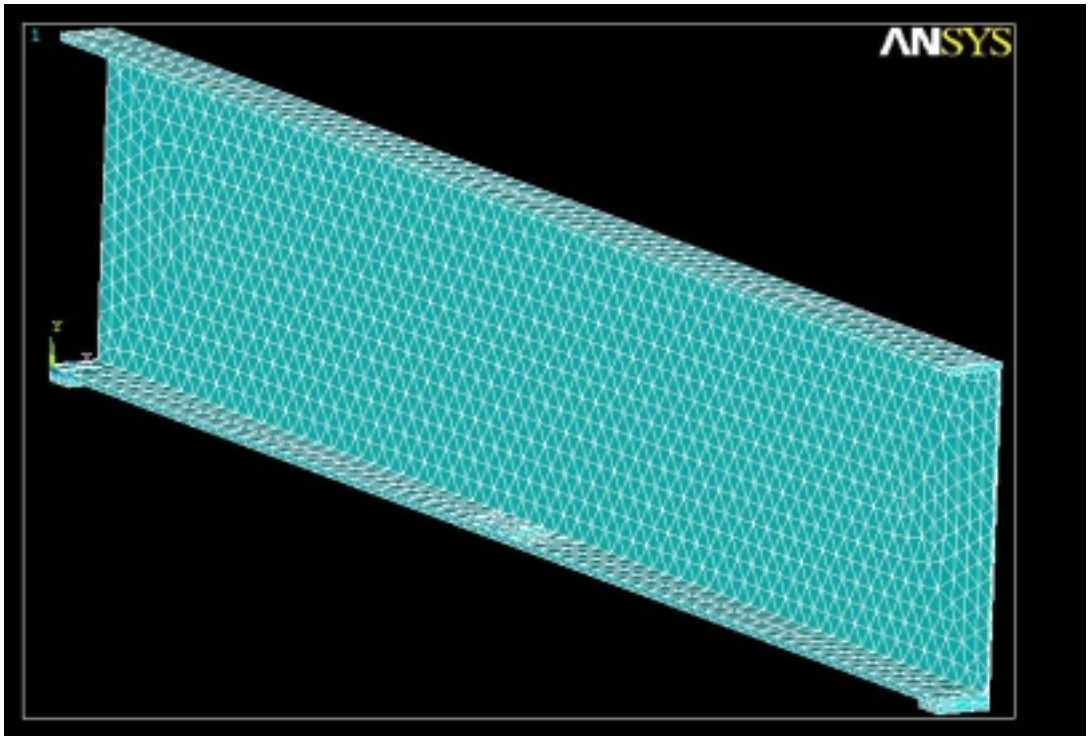

FIGURE 3-4. Finite Element Model

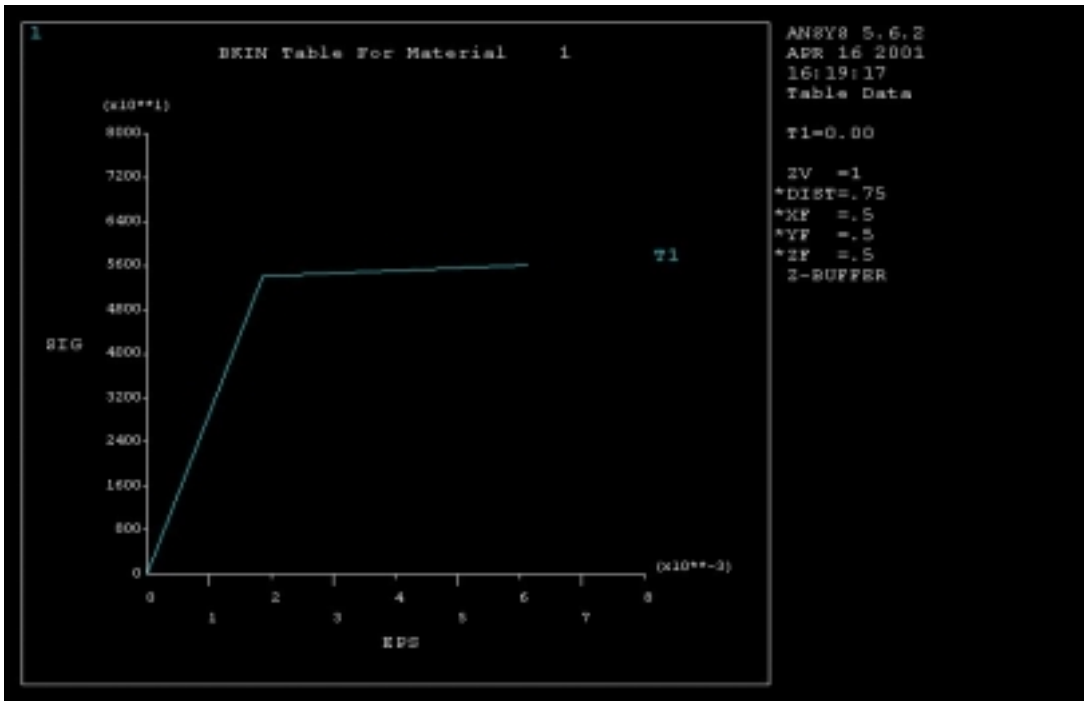

FIGURE 3-5. Stress-strain Behavior for ANSYS Models

3.2.2 LOAD AND BOUNDARY CONDITIONS

The models were assumed to be simply supported in plane, i.e., the ends are fixed against in-plane vertical deflection but unrestrained against in-plane rotation. In addition, one end is fixed against longitudinal horizontal displacement. Symmetry about the vertical axis was used to reduce the analysis time of the girder models. A surface vertical load is applied incrementally to the ½ in. thick steel plate located in the middle section of the girder models. Two additional ½ in. thick plates were added at both ends to represent the actual simply supported condition experienced by the girders. Nodes along the symmetrical surface are fixed against lateral translation (x-direction) and rotation about the y- and z- axes.

3.2.3 ANSYS MODELS

The ANSYS models are used to validate the experimental results. It is assumed that the fillet volume of the sections is insignificant and therefore is ignored in ANSYS. It is also assumed that the distributed load via the bearing plate in ANSYS reflects the actual load conditions during the testing phase, i.e., Options A and B.

The total load vs. midspan deflection behavior for the five ANSYS girder models is illustrated in Figure 3-6. A constant girder span of 96 in. was used for all five models with a total applied load of 224 kips. This constant length is used only in comparing the ANSYS results to determine the level of consistency between the models. The actual girder length of 78 or 96 in. is used otherwise, namely when comparing with experimental results in Chapter Four. The larger the section, the stiffer the section behaves as the girder deflects, as expected. It is interesting to note that the W18x40 section becomes very flexible relative to the other four girders as the section approaches the total load applied.

The total load vs. relative deflection plot for the five models is shown in Figure 3-7. The behavior of the models is fairly consistent, with the largest relative deflection being the W24x68 section. This is expected because it has the largest flange width (similar to a cantilever beam case) and therefore, given the same load, will exhibit the largest relative deflection.

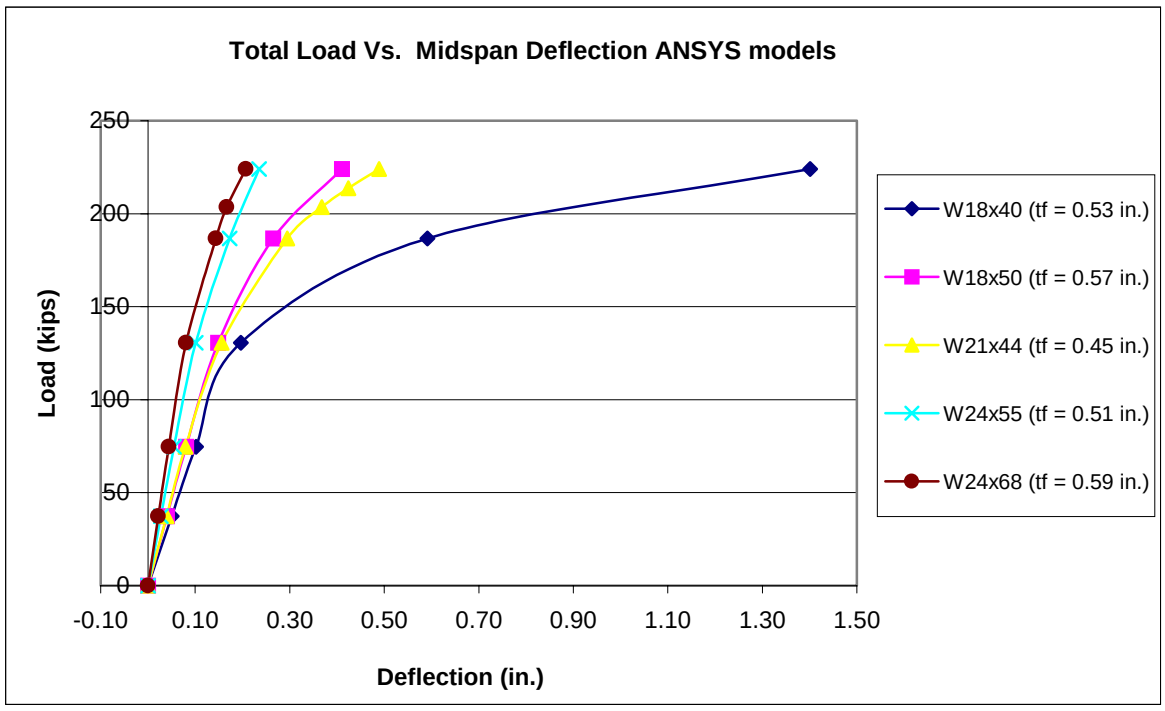

FIGURE 3-6. Total Load vs. Midspan Deflection Plot of ANSYS Models

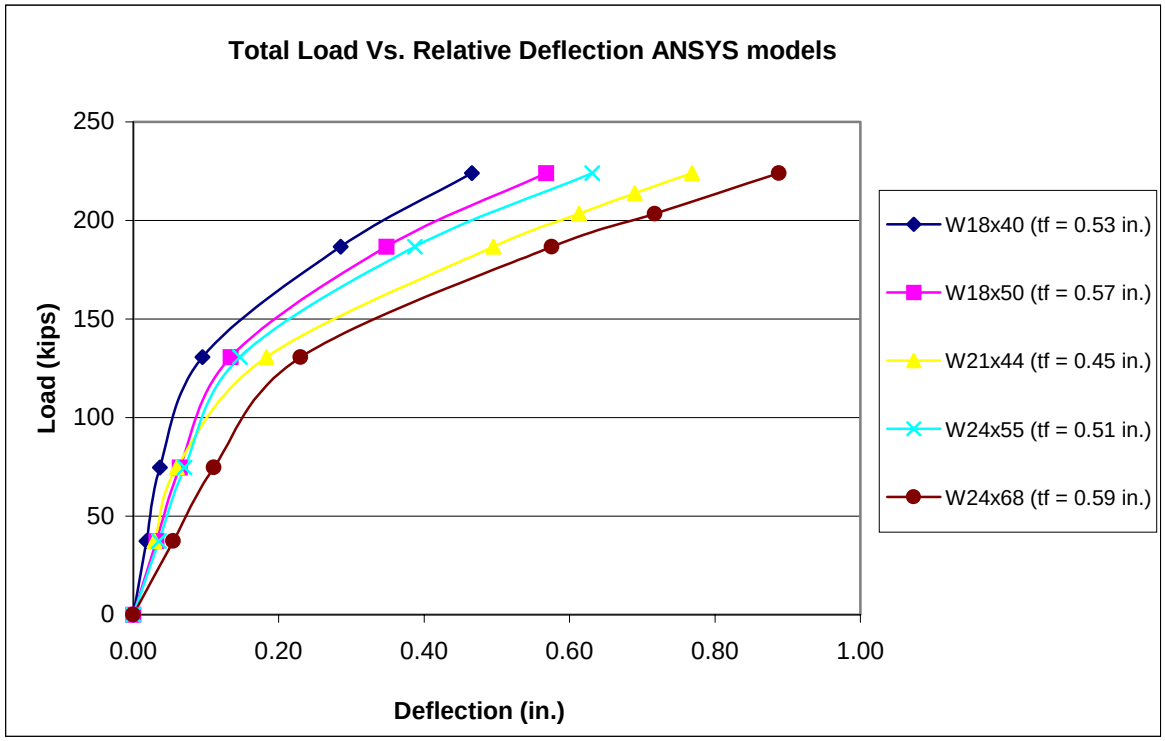

FIGURE 3-7. Total Load vs. Relative Deflection Plot of ANSYS Models

3.2.4 STRESS FIELD IN MODELS

Figure 3.8 through Figure 3-10 are different views of the stress field as a result of the load being applied as the section approaches first yielding. All five models developed similar stress field patterns. The stress field patterns show a consistent flow of stresses as anticipated from the area of applied load and throughout the girder length. Maximum stresses were found to be in the vicinity between the bottom flange and girder web as shown below. It is also noted that the stress field depicts a similar fan-like pattern to that of the yield line pattern, which was used to derive the proposed yield line equation.

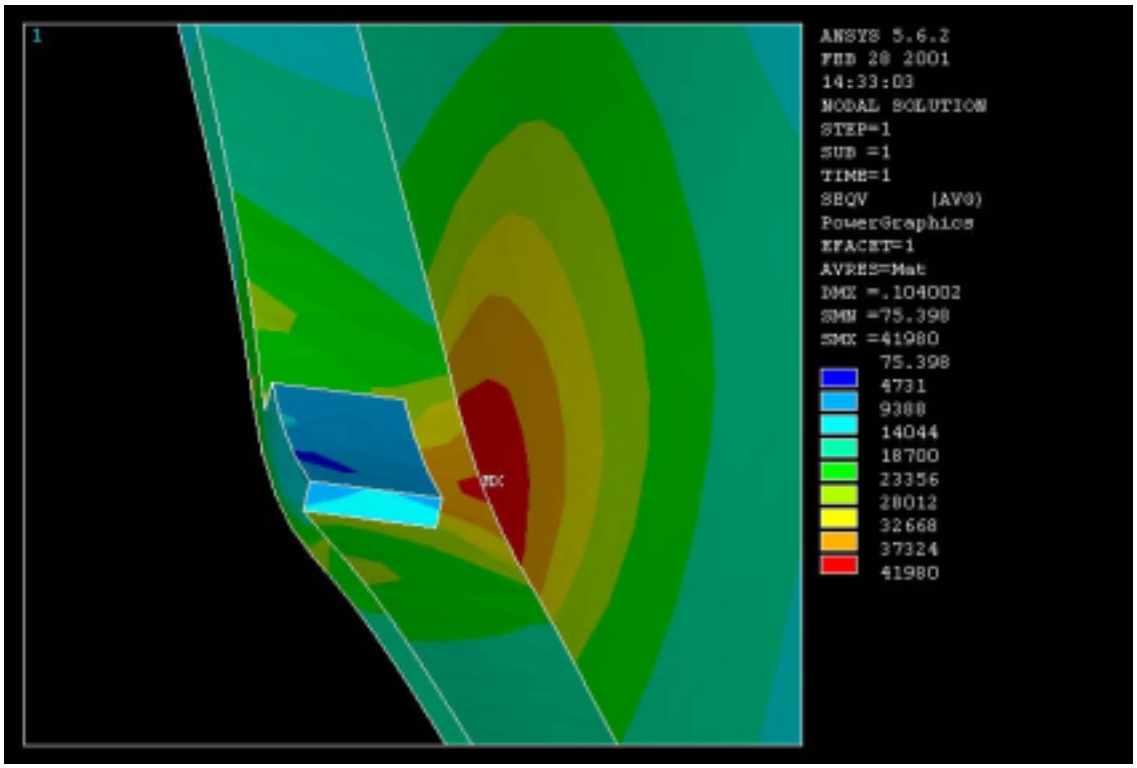

FIGURE 3-8. Stress Field View for W21x44 Model

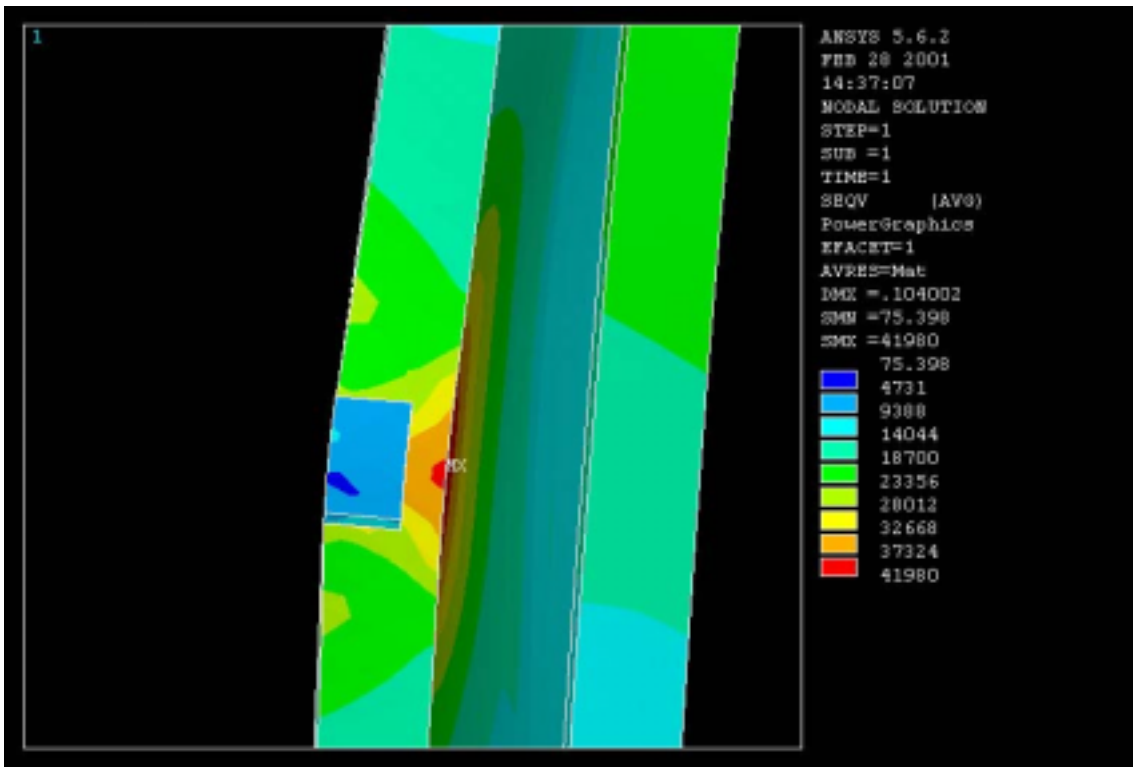

FIGURE 3-9. Stress Field Top View for W21x44 Model

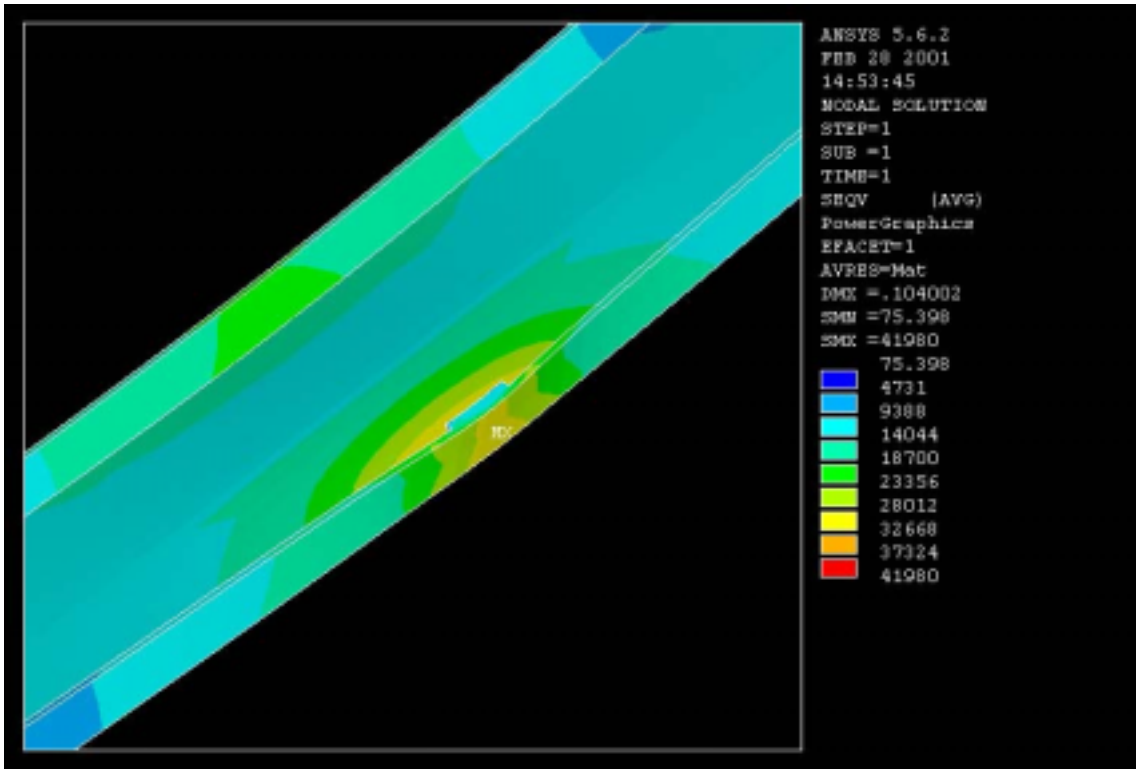

FIGURE 3-10. Stress Field Bottom View for W21x44 Model

3.2.5 COMPARISON OF W24X68 MODEL WITH BOLT HOLES

To model the beam-to-girder connection behavior with the presence of holes in the girder flanges, an analysis was conducted using two standard ¾" bolt holes. The modified section was then compared to the ANSYS model as shown below in the total load vs. relative deflection plot (Fig. 3-11). The W24x68 model was chosen simply because of its good initial results when compared to its counterpart in the testing program. The same load conditions, as well as section and material properties, are used in both cases. As seen below, the results show little difference in relative deflection behavior between the two models as load is being applied. The reason is that the bolt holes are within the beam bearing area (plate) and the inclusion of the two bolt holes causes insignificant changes in relative deflection, as expected.

Figures 3-12 and 3-13 illustrate the stress field in the W24x68 model with the bolt holes. The stress field appears irregular around the applied load area compared to the previous models as a result of the inclusion of the two bolt holes. This is expected, as the holes will induce high stresses because of their irregularity.

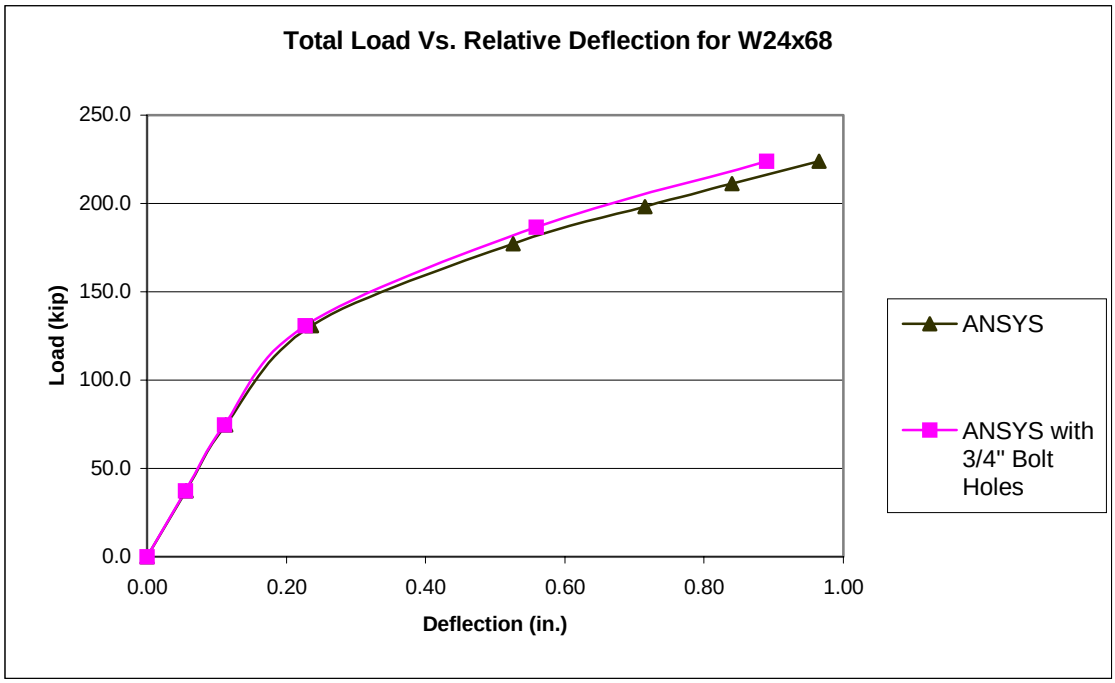

FIGURE 3-11. Total Load vs. Relative Deflection for W24X68 Model with Bolt Holes

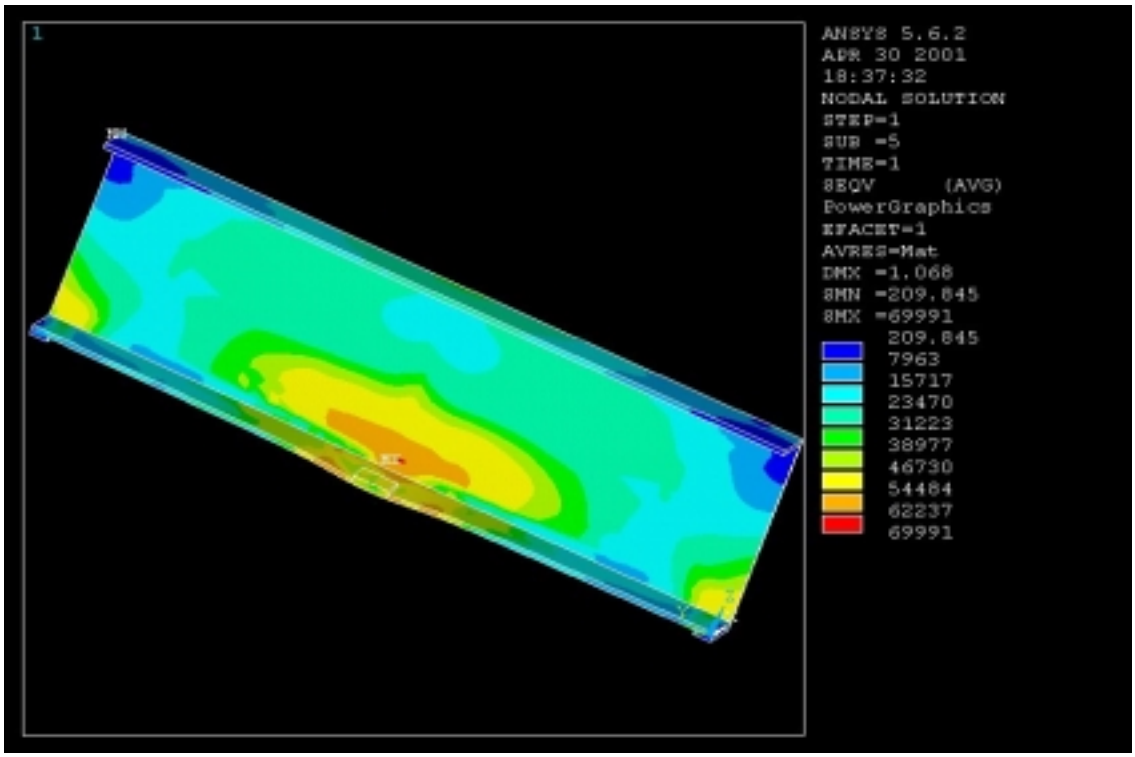

FIGURE 3-12. Stress Field View for W24X68 Model with Bolt Holes

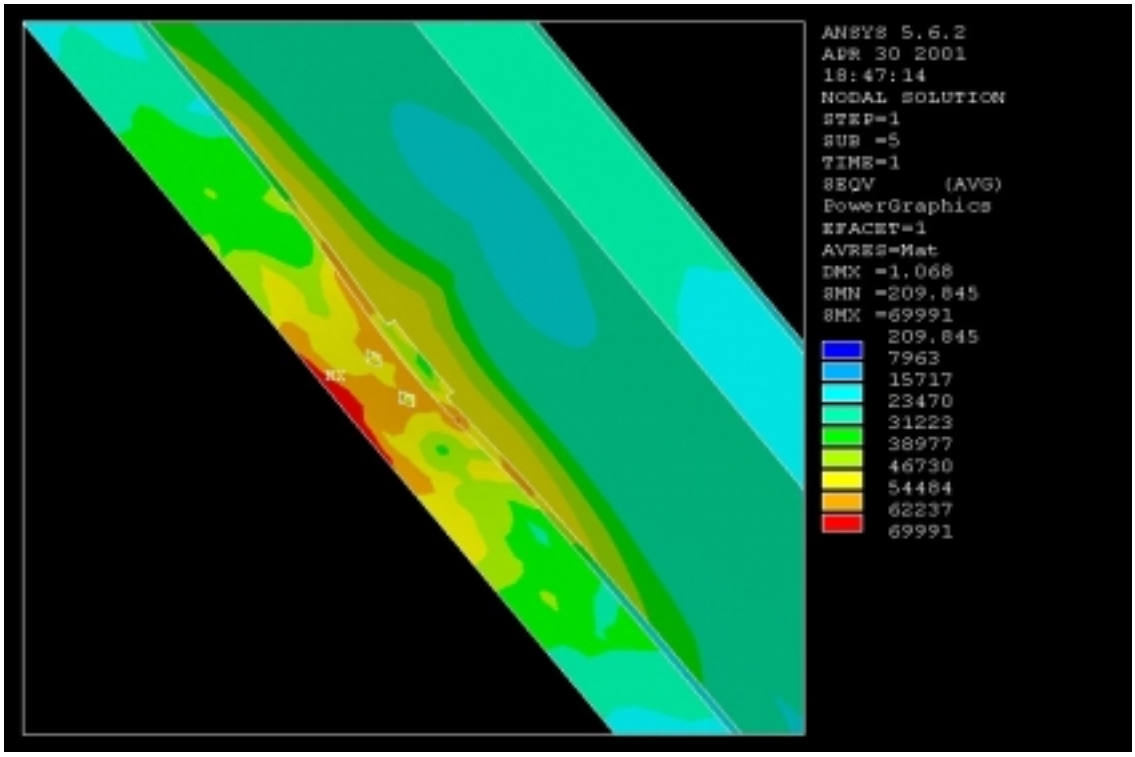

FIGURE 3-13. Stress Field Bottom View for W24X68 Model with Bolt Holes

3.2.6 COMPARISON OF W24X68 MODEL WITH ONE-SIDED LOAD

This research also looks into the case where the same W24x68 model is applied with a single-sided load. A full girder model and simply supported condition were used. The configuration models an exterior beam-to-girder connection. The one-sided load model was loaded until 147 kips and compared with the W24x68 model with both sides being loaded equally. The one-sided load case resulted in a higher relative deflection for a given load, particularly after first yield (Fig. 3-14). However, it does show consistent behavior in the elastic portion. This is because for a given deflection, less work is done in a one-sided load case compared to both sides being equally loaded. Figure 3-15 depicts the stress field pattern of the one-sided load model. It shows similar fan-like stress patterns as shown previously in the initial models.

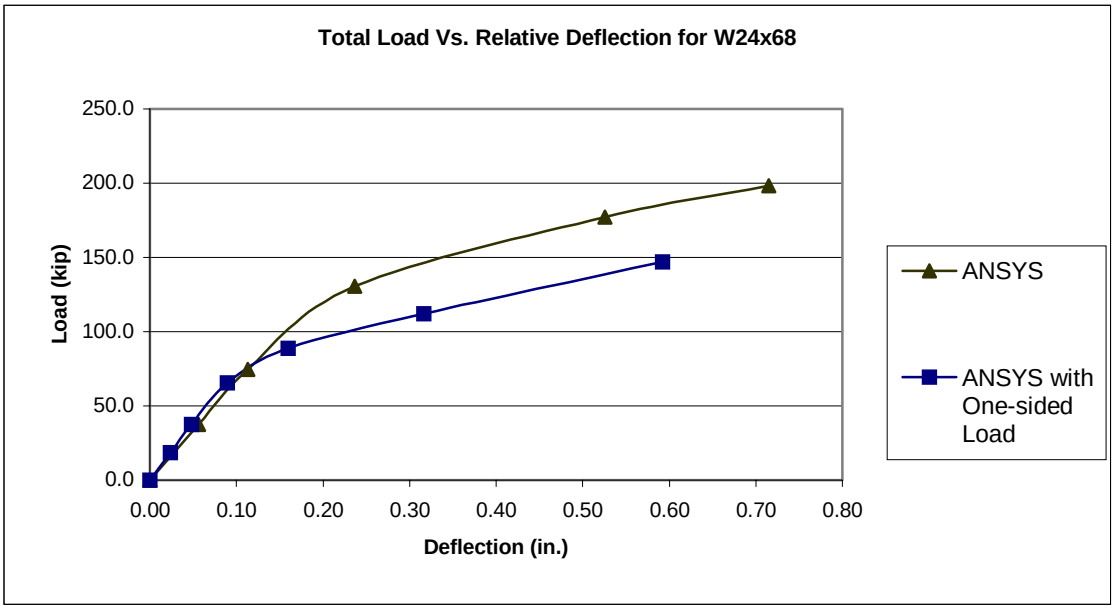

FIGURE 3-14. Load vs. Relative Deflection for W24X68 Model with One-Sided Load

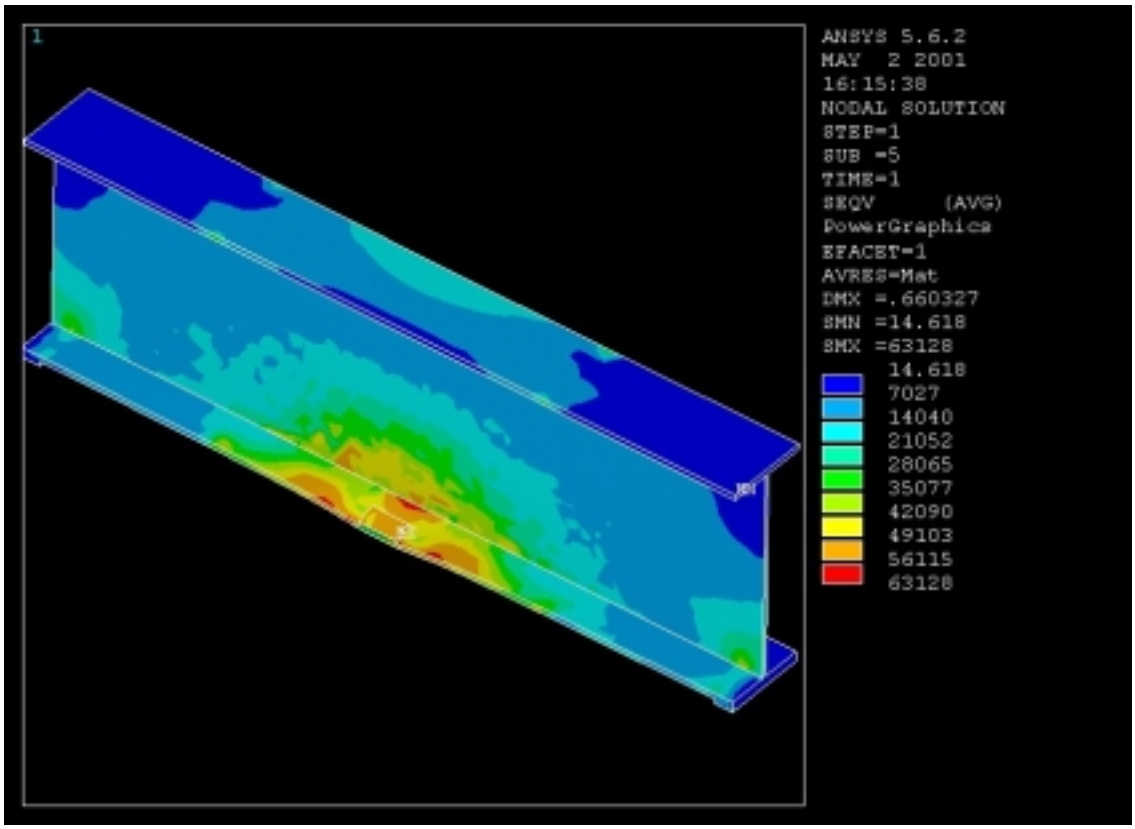

FIGURE 3-15. Stress Field View for W24X68 Model with One-Sided Load

CHAPTER FOUR
COMPARISON BETWEEN EXPERIMENTAL AND ANALYTICAL RESULTS

4.1 COMPARISON OF TOTAL LOADS

The total load and moment values from the testing phase and ANSYS results are presented in Table 4-1. The estimated load at first yield from the proposed yield line equation, R_{yield}, is also shown for comparison. M_{app} is the moment due to the applied load $R_{app,}$ which is obtained from finding the intersection of two straight lines in a load vs. deflection plot from the testing phase. An example of this technique is shown in Figure 4-1. R_{ansys} is obtained likewise from the load vs. deflection plots from the ANSYS results. M_p is the plastic moment of the section that corresponds to the actual yield stress of the particular girder. It is noted that the differences between the experimental and analytical loads from the proposed yield line equation R_{yield} were found generally to be larger as the size of the section increases. The five load and moment values of each section are compared in Table 4-2. It is noted that the W18x40 section approaches its plastic moment limit whereas the W21x44 section is only at 27 percent of its plastic moment strength.

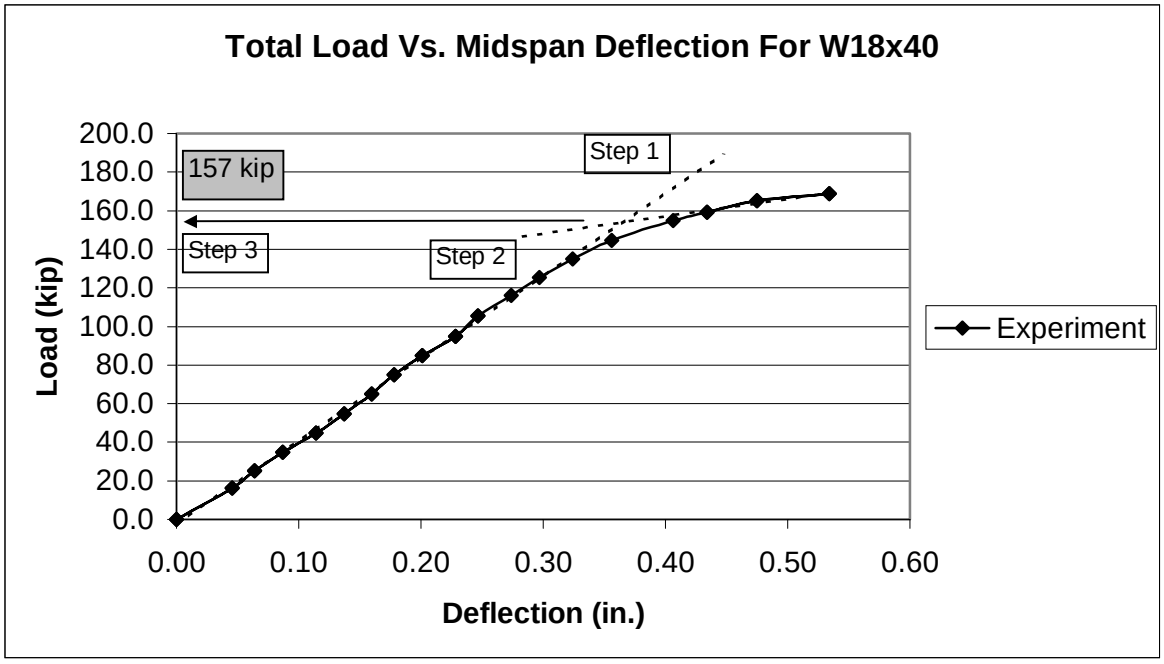

FIGURE 4-1. Steps to Obtain the Applied Load, R_{app}

The range of the ratios varies substantially from one-half to two and does not indicate any particular trend. However, when comparing both R_{yield} and $R_{ansys,}$ the proposed equation seemed to be giving a smaller range of ratio values, varying between 0.57 and 0.88. R_{yield} is found to be conservative compared to $R_{app.}$ However, note that R_{app} is the applied load where the first yielding occurs and is lower than the ultimate load of the particular girder section. As a result, the proposed yield line equation can be used to predict the applied load at first yielding.

TABLE 4-1. Total Load and Moment Values from Experiment, Proposed Yield Line Equation and ANSYS Results

Section	R_{app} (kips)	R_{yield} (kips)	R_{ansys} (kips)	M_{app} (kips*in)	M_p (kips*in)
W18x40	157	88	125	3768	3976
W18x50	124	108	146	2418	5543
W21x44	58	68	116	1392	5153
W24x55	90	94	129	2160	7822
W24x68	234	113	128	4563	9427

TABLE 4-2. Comparison of Actual, Proposed Yield Line Equation and ANSYS Results

Section	M_{app}/M_p	R_{app}/R_{yield}	R_{app}/R_{ansys}	R_{yield}/R_{ansys}
W18x40	0.95	1.78	1.26	0.70
W18x50	0.44	1.15	0.85	0.74
W21x44	0.27	0.88	0.50	0.57
W24x55	0.28	0.98	0.70	0.71
W24x68	0.48	2.09	1.83	0.88

4.2 COMPARISON OF TOTAL LOAD VS. DEFLECTION PLOTS

The behavior of the sections both analytically and experimentally is compared via the load vs. relative deflection plot. The relative deflection denotes the difference between the edge deflection and the deflection at midspan due to bending alone. This is done in order to capture the effects of the load being applied at the local level. All five girders were found to be short enough (slenderness ratio < 10) to result in significant shear deformations (Table 4-3). Timoshenko (1958) outlined a deflection equation to approximate the contribution of shear deformations in addition to bending as follows:

$$\delta = \frac{Pl^3}{48EI_x} + \frac{\alpha}{AG}\left(\frac{Pl}{4}\right) \tag{4.1}$$

where $\alpha = \frac{A}{t_w I_x}\left[\frac{b_f D^2}{8} + \frac{(D-2t_f)^2(b_f - t_w)}{8}\right]$ (4.2)

D = depth of section

I_x = moment of inertia (x-axis)

G = shear modulus of steel = 11,200 ksi

A = cross sectional area of girder

TABLE 4-3. Slenderness Ratio of the Five Girder Sections

Section	Span (in.)	D/L Ratio
W18x40	96	5.36
W18x50	78	4.34
W21x44	96	4.65
W24x55	96	4.07
W24x68	78	3.29

The theoretical deflection, which includes the effect of bending and shear deformations, is used to validate the five finite element models. It is found that the theoretical deflections correlate well in the elastic portion with the deflections obtained from the finite element study. The ANSYS models in general show a stiffer section compared to the experimental results, as expected. This is because the finite element models will experience less work being done for the same loading as a result of the element mesh compared to the continuum models, which are the experimental results. Figures 4-1 to 4-10 show the total load vs. midspan and relative deflection plots for each of the five girder sections.

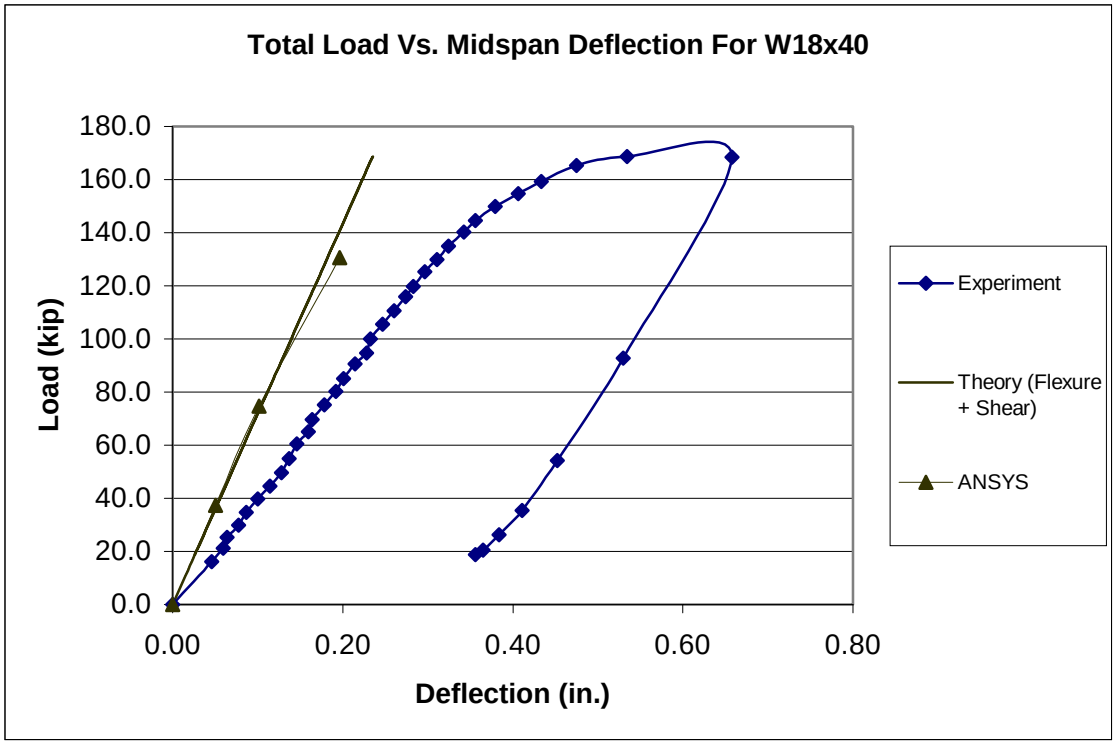

FIGURE 4-2. Load vs. Midspan Deflection Plot for W18x40

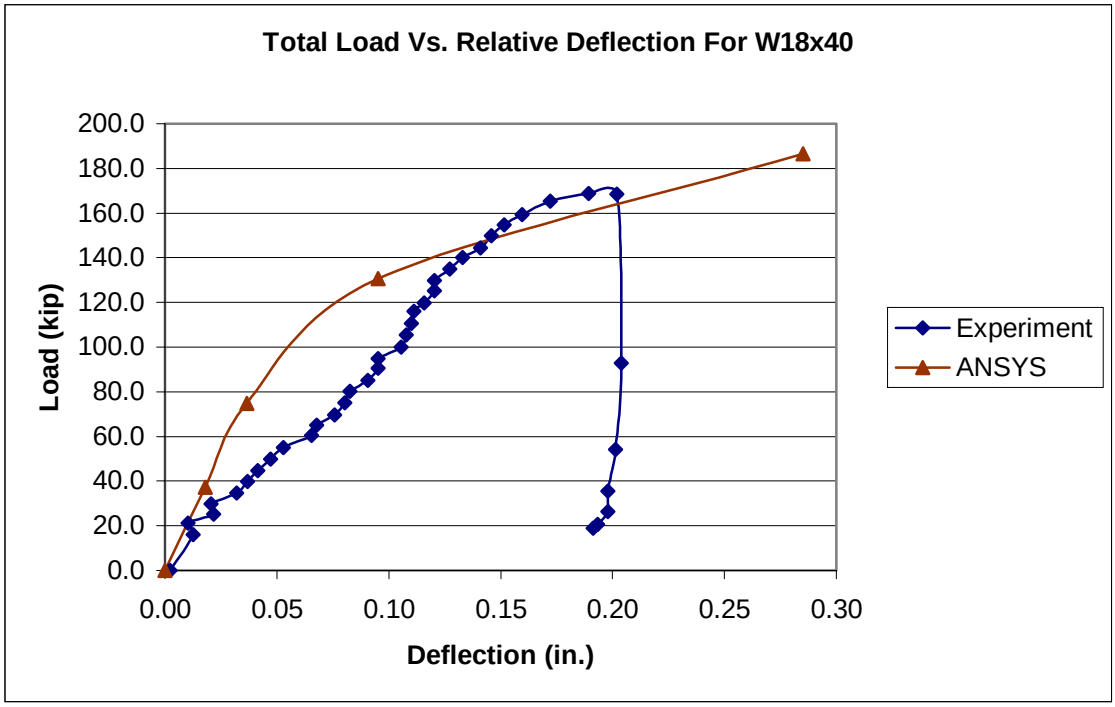

FIGURE 4-3. Load vs. Relative Deflection Plot for W18x40

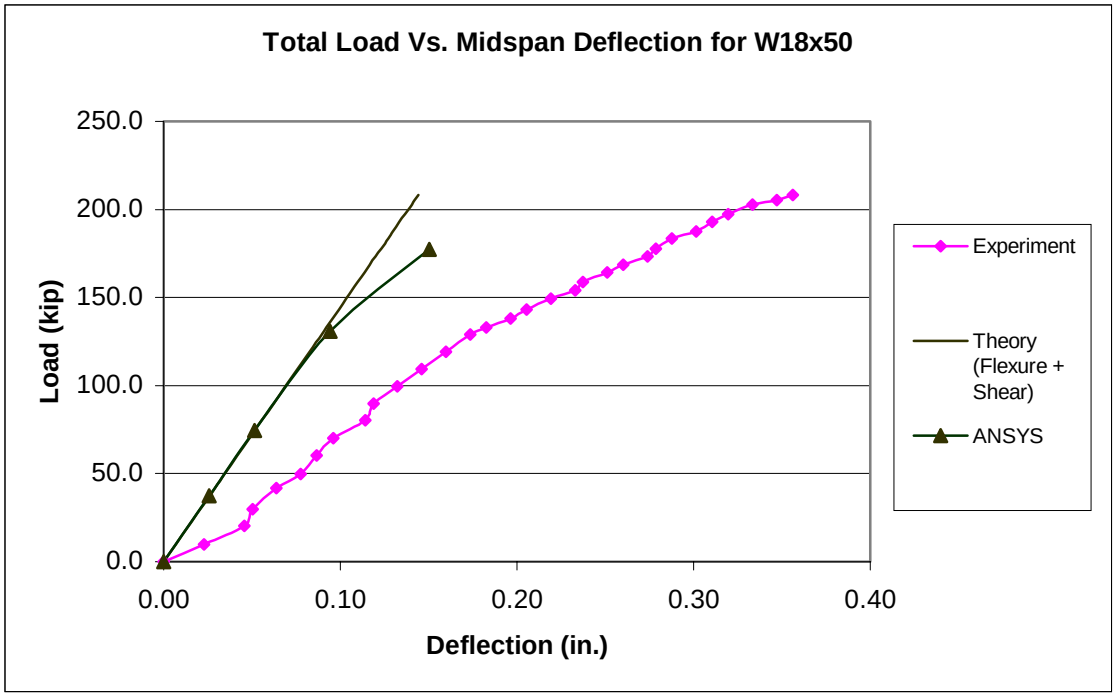

FIGURE 4-4. Load vs. Midspan Deflection Plot for W18x50

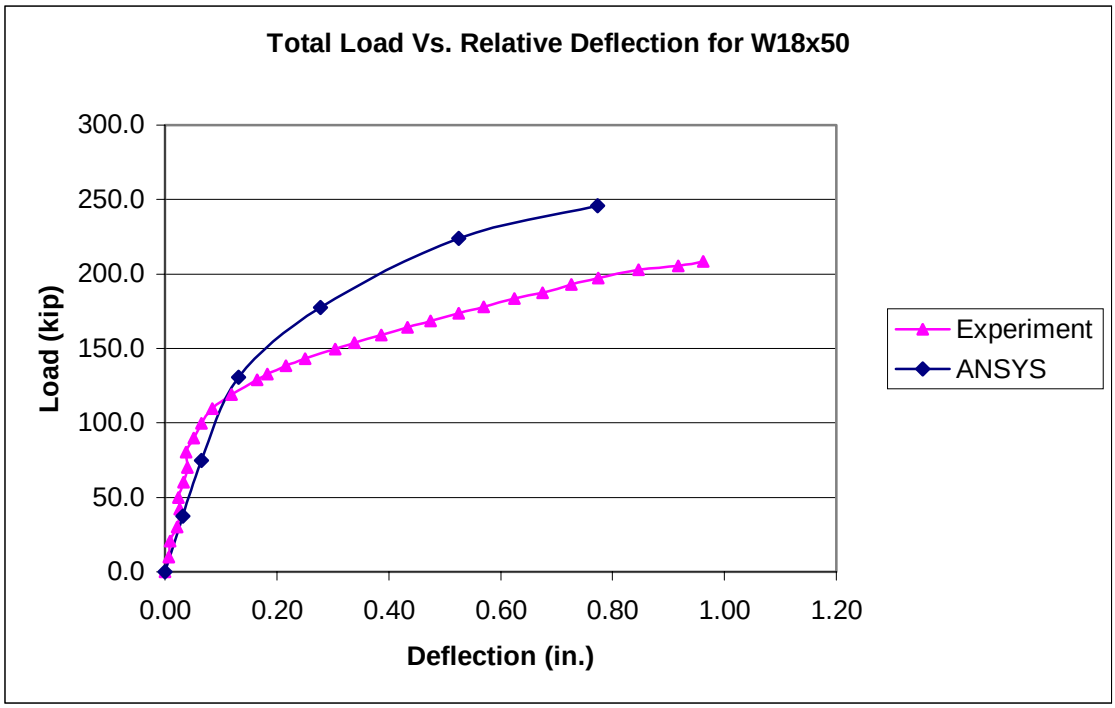

FIGURE 4-5. Load vs. Relative Deflection Plot for W18x50

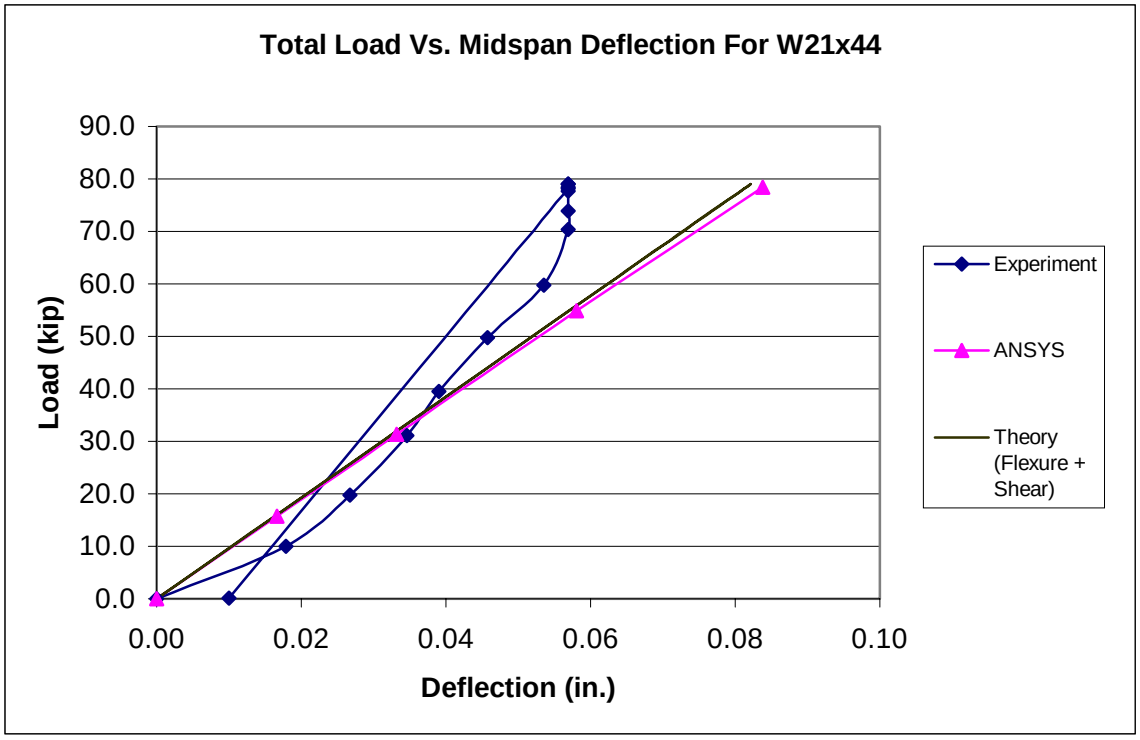

FIGURE 4-6. Load vs. Midspan Deflection Plot for W21x44

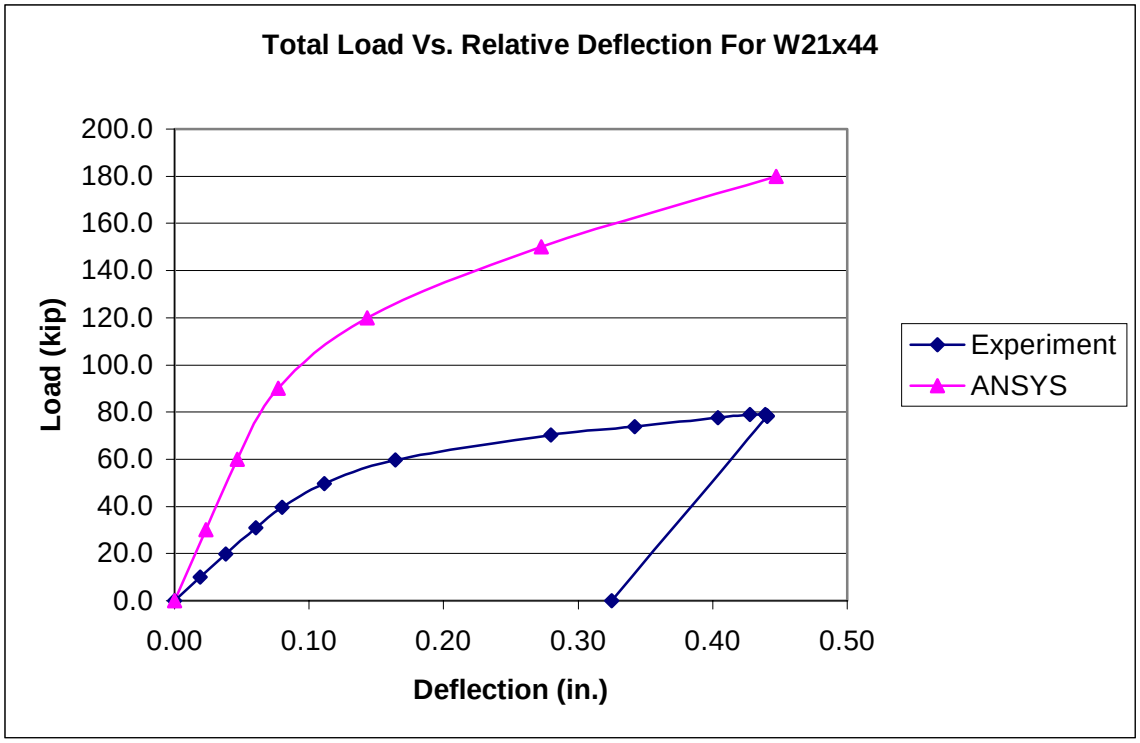

FIGURE 4-7. Load vs. Relative Deflection Plot for W21x44

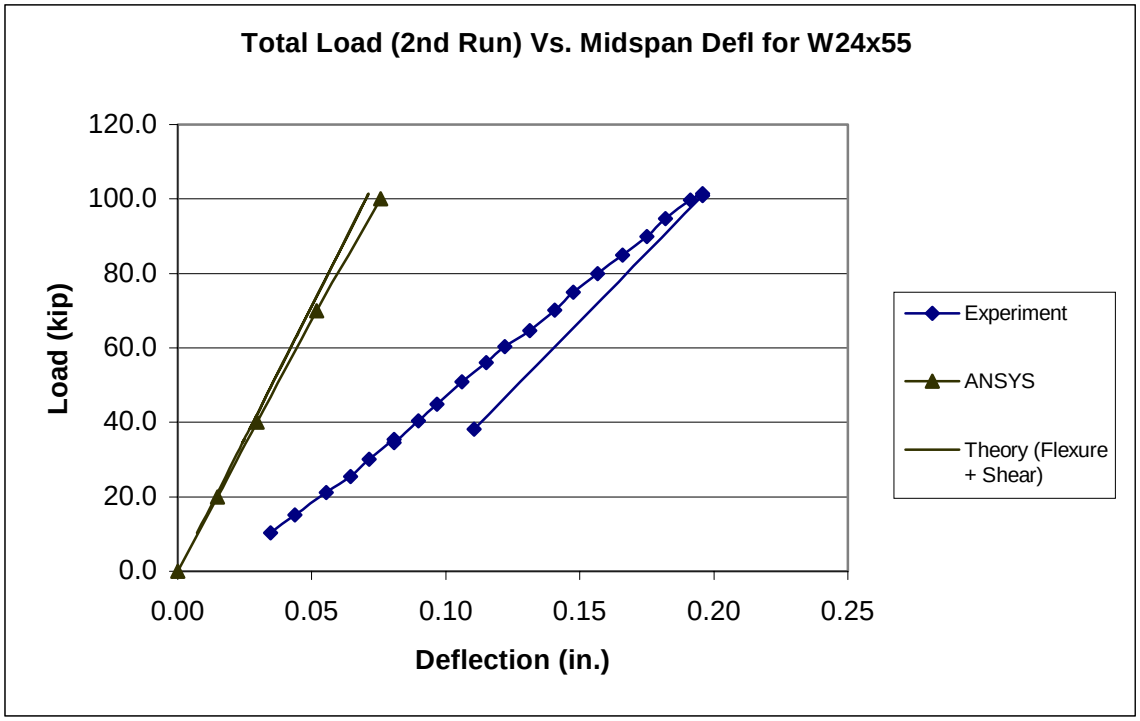

FIGURE 4-8. Load vs. Midspan Deflection Plot for W24x55

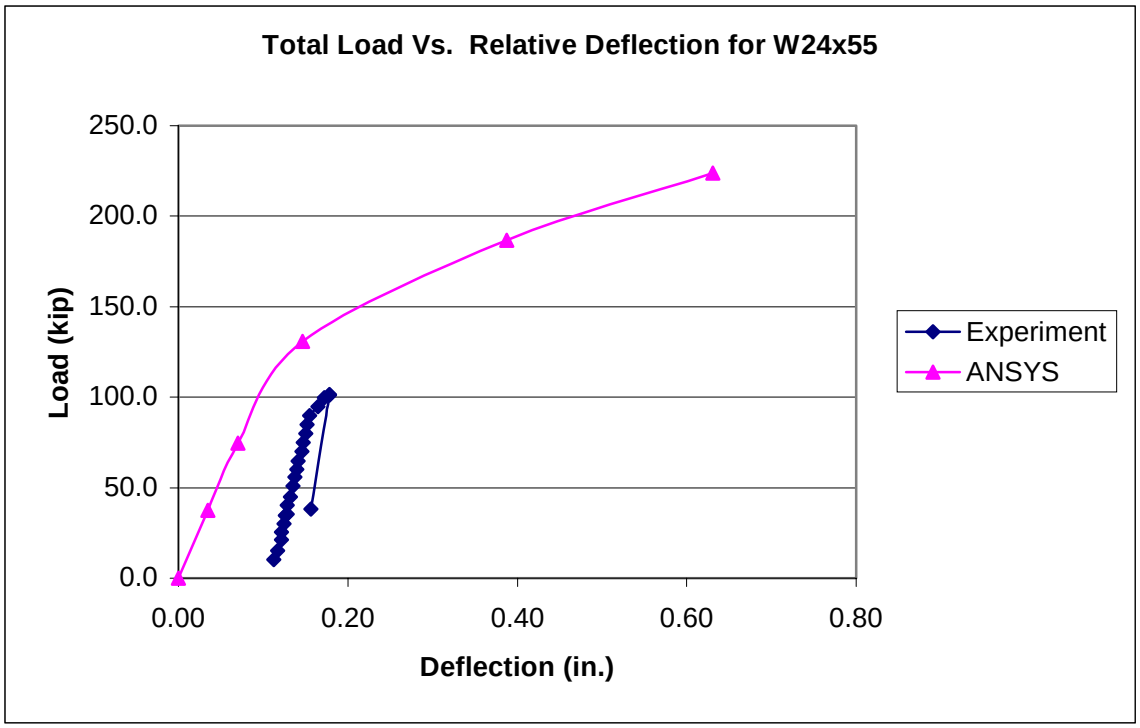

FIGURE 4-9. Load vs. Relative Deflection Plot for W24x55

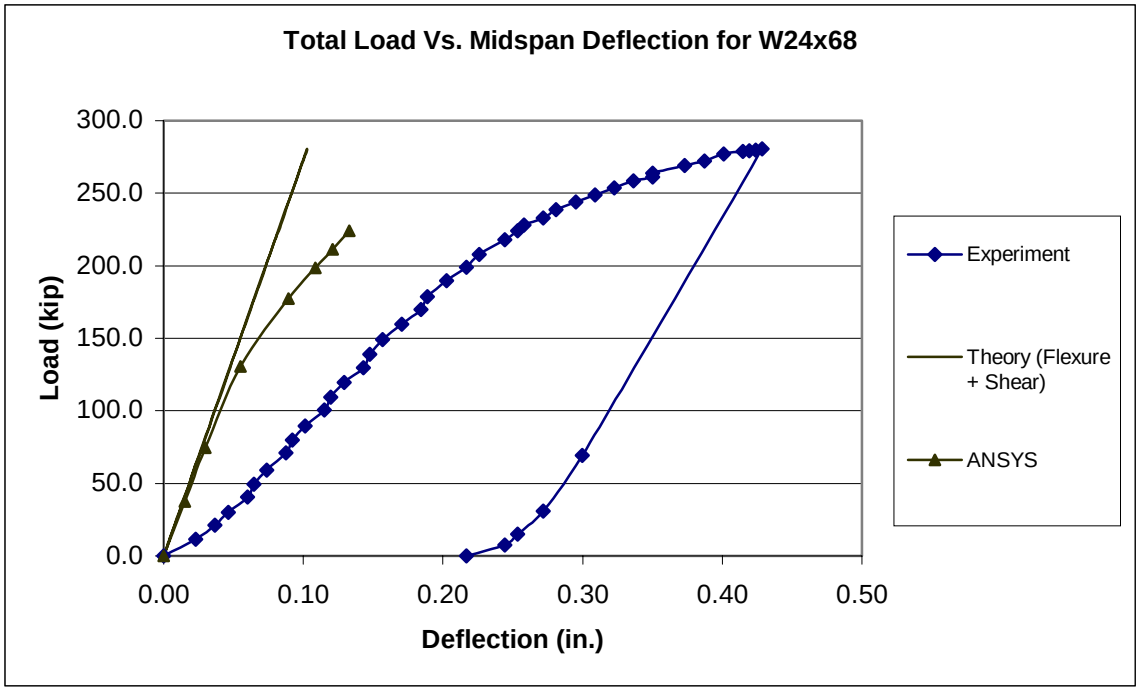

FIGURE 4-10. Load vs. Midspan Deflection Plot for W24x68

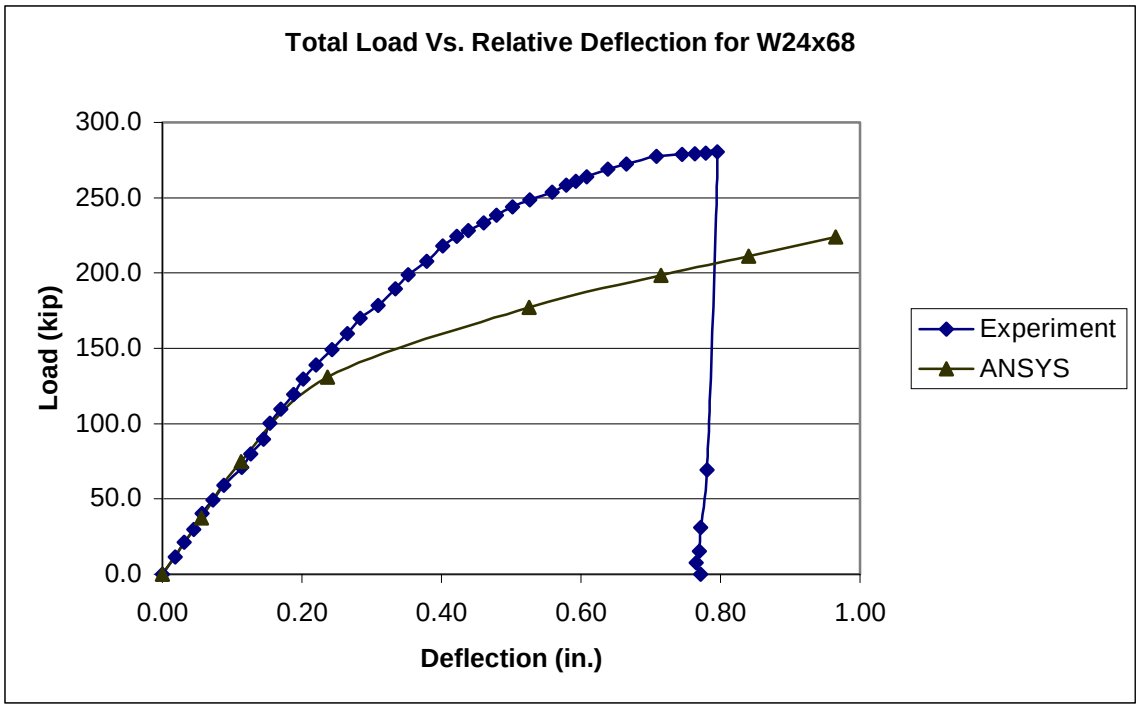

FIGURE 4-11. Load vs. Relative Deflection Plot for W24x68

4.3 COMPARISON OF STRAIN AND STRESS VALUES

To verify the experimental results, strain readings were compared to the ANSYS output. Referring to the setup and location of the gages, the six gages were categorized into three main groups using symmetry as tabulated in Tables 4-4 to 4-6. Strain values were picked at random load steps. The principal strains ε_1 and ε_3 correspond to the maximum and minimum strains, respectively. The principal experimental strains are obtained by taking into account the layout and arrangement of the strain gages during the testing program.

TABLE 4-4. Strain Values Comparison at Gage Location 1 and 2 (Average)

Section	Load (kips)	Experimental Strains		ANSYS Strains	
		Principal Strain, ε1	Principal Strain, ε3	Principal Strain, ε1	Principal Strain, ε3
W18x40	37.3	0.001951	-0.003703	0.000555	-0.000373
	74.7	0.006613	-0.004032	0.001136	-0.000754
	130.7	0.013717	-0.002082	0.001307	-0.001241
W18x50	37.3	0.000401	-0.000512	0.000511	-0.000142
	74.7	0.000593	-0.000653	0.000913	-0.000345
	130.7	0.001291	-0.000691	0.001123	-0.000898
W21x44	30.0	0.000203	-0.001396	0.000575	-0.000827
	60.0	0.000580	-0.001808	0.001112	-0.001619
W24x55	37.3	0.000782	-0.002645	0.000698	-0.000196
	74.7	0.004861	-0.007097	0.001363	-0.000351
W24x68	37.3	0.002246	-0.000564	0.000314	-0.000056
	74.7	0.007738	-0.000372	0.000676	-0.000118
	130.7	0.014700	-0.001859	0.000830	-0.000292

TABLE 4-5. Strain Values Comparison at Gage Location 3 and 6 (Average)

Section	Load (kips)	Experimental Strains		ANSYS Strains	
		Principal Strain, ε1	Principal Strain, ε3	Principal Strain, ε1	Principal Strain, ε3
W18x40	37.3	0.000918	-0.000007	0.000546	-0.000120
	74.7	0.001718	-0.000065	0.001013	-0.000242
	130.7	0.002610	-0.000157	0.001075	-0.000348
W18x50	37.3	0.000534	-0.000045	0.000626	-0.000011
	74.7	0.000900	-0.000078	0.000995	-0.000059
	130.7	0.005589	-0.000923	0.003246	-0.000121
W21x44	30.0	0.000971	-0.000009	0.000744	-0.000026
	60.0	0.004135	-0.000831	0.001223	-0.000052
W24x55	37.3	0.000664	-0.000023	0.000518	-0.000118
	74.7	0.001383	-0.000089	0.001259	-0.000149
W24x68	37.3	0.000670	-0.000071	0.000189	-0.000242
	74.7	0.001429	-0.000181	0.000377	-0.000489
	130.7	0.002889	-0.000536	0.000797	-0.001125

TABLE 4-6. Strain Values Comparison at Gage Location 4 and 5 (Average)

Section	Load (kips)	Experimental Strains		ANSYS Strains	
		Principal Strain, ε1	Principal Strain, ε3	Principal Strain, ε1	Principal Strain, ε3
W18x40	37.3	0.001570	-0.000147	0.000578	-0.000141
	74.7	0.004260	-0.000381	0.001236	-0.000347
	130.7	0.009891	-0.000690	0.001172	-0.000558
W18x50	37.3	0.000546	-0.000065	0.000691	-0.000042
	74.7	0.000955	-0.000130	0.001095	-0.000086
	130.7	0.005439	-0.001351	0.003601	-0.000327
W21x44	30.0	0.000774	-0.000023	0.000848	-0.000078
	60.0	0.003276	-0.000478	0.001565	-0.000102
W24x55	37.3	0.000852	-0.000035	0.000792	-0.000092
	74.7	0.001839	-0.000161	0.001511	-0.000191
W24x68	37.3	0.000878	-0.000143	0.000284	-0.000233
	74.7	0.001878	-0.000349	0.000476	-0.000539
	130.7	0.004447	-0.000847	0.000924	-0.001246

*__Note__: W21x44 does not have strain data at loads above total load of 80 kips while W24x55 is being loaded cyclically, thus strain data are not accurate after the 1st run of loading.

Bending stresses in the ANSYS models are verified with the theoretical values in the elastic range. For girder sections at 96-inch span, stresses are calculated and compared at the 16-in. and 32-in. lengths away from the support edge, while for the sections at 78-in. span, the stresses are obtained at 12-in. and 24-in. lengths away from the support edge. In all five cases, a constant total load of 72 kips is applied in the ANSYS models. The theoretical stresses correlate well with the ANSYS results in all five sections as tabulated in Table 4-7 below.

TABLE 4-7. Stress Values Comparison Of ANSYS Models

Section	Location Along Beam From Support Edge (in.)	Theoretical Stress Value (psi)	ANSYS Stress Value (psi)
W18x40	16 32	8424 16847	7556 15494
W18x50	12 24	4860 9720	5147 10791
W21x44	16 32	7058 14116	6664 13467
W24x55	16 32	5030 10061	5312 9909
W24x68	12 24	2802 5604	4550 7495

CHAPTER 5
DESIGN PROCEDURE

5.1 RESULTS OF THE YIELD LINE EQUATION

A design procedure based on the proposed yield line equation is presented in this chapter. The results from the equation based on section properties of various beam and girder shapes are shown in Table 5-1. The beams are picked so that they are usually a shape smaller than the corresponding girder. A yield stress of 50 ksi and several beam bearing (flange) widths are considered for each girder section. Reaction values for a load case of a girder with two equal loads (one on each side) and for a load case of a girder with one load are also presented below. It is noted that there is a need for more full-scale testing of similar sections in order to develop the resistance factor through a probability study for the proposed equation. Hence, the resistance factor is omitted here till a more comprehensive testing program can be done.

TABLE 5-1. Load Reaction Comparison of Girder Sections

Input										Total Load at Both Sides	Total Load at One Side
Beam	b_{fb} (in)	Girder	F_y (ksi)	b_{fg} (in)	k_1 (in)	t_w (in)	b_{fg} (in)	N (in)	t_f (in)	R_n (kips)	R_n (kips)
W16	5.5	W18x40	50.0	6.015	0.813	0.315	2.195	1.445	0.525	84	42
	7.0		50.0	6.015	0.813	0.315	2.195	1.445	0.525	91	45
W16	5.5	W18x50	50.0	7.495	0.813	0.355	2.935	2.185	0.570	97	49
	7.0		50.0	7.495	0.813	0.355	2.935	2.185	0.570	104	52
W18	6.0	W21x44	50.0	6.500	0.875	0.350	2.375	1.625	0.450	63	31
	7.5		50.0	6.500	0.875	0.350	2.375	1.625	0.450	68	34
	11.0		50.0	6.500	0.875	0.350	2.375	1.625	0.450	79	40
W21	6.5	W24x55	50.0	7.005	0.938	0.395	2.565	1.815	0.505	81	40
	8.5		50.0	7.005	0.938	0.395	2.565	1.815	0.505	89	44
W21	6.5	W24x68	50.0	8.965	0.938	0.415	3.545	2.795	0.585	106	53
	8.5		50.0	8.965	0.938	0.415	3.545	2.795	0.585	114	57

5.2 DESIGN EXAMPLE

Consider a typical office floor bay with a live load of 70 psf and a dead load of 70 psf. Two beams are spaced symmetrically at 10 feet apart on a 30-feet girder. The beams are 35 feet in length. Beam weight is estimated to be 50 plf. A load case will be considered with a girder loaded at one side (exterior case).

W_L = 10 (60) = 0.60 k/ft

W_D = 10 (70) + 50 = 0.75 k/ft

$$Wu = \max\begin{Bmatrix} 1.4W_D = 1.05k/ft \\ 1.2W_D + 1.6W_L = 1.86k/ft \rightarrow controls \end{Bmatrix}$$

Applied load, $R_U = \frac{wl}{2} = \frac{1.86(35)}{2} = 32.6kips$

$$M_U = \frac{wl^2}{8} = \frac{1.86(35^2)}{8} = 284.8kft$$

$$Z_R = \frac{M_U}{0.9F_y} = \frac{284.8(12)}{0.9(50)} = 76.0in^3$$

Pick beam W21x44, $Z_x = 95.4\ in^3 > 76.0\ in^3$ OK

d = 20.7 in. > $\frac{35'}{2}$ = 17.5 in. Deflection probably OK

Check Compactness: $\lambda \le \lambda_p$

W21x44 section properties: b_f = 6.5 in., k = 1.188", t_f = 0.45 in., t_w = 0.35 in.

W21x44: $\lambda_{flg} = 7.2 < \lambda_p = \frac{65}{\sqrt{50}} = 9.2$ OK

$\lambda_{web} = 53.6 < \lambda_p = \frac{640}{\sqrt{50}} = 90.5$ OK

Check Local Web Yielding of the Beam:

Section K1-3, Manual of Steel Construction LRFD, Volume 1:

$\phi = 1.0$ and $R_n = 1.0 (N + 2.5 k) F_{yw} t_w$ (K1-3)

N = 1.82 in. (from Table 5-1)

Therefore, $\phi R_n = 83.8$ kips > Ru = 32.6 kips OK

Check Web Crippling of the Beam:

Section K1-4, Manual of Steel Construction LRFD, Volume 1:

Since $\frac{N}{d} \leq 0.2$,

$\phi = 0.75$ and $R_n = 68 t_w^2 \left[1 + 3\left(\frac{N}{d}\right)\left(\frac{t_w}{t_f}\right)^{1.5}\right]\sqrt{\frac{F_{yw} t_f}{t_w}}$ (K1-5a)

$\phi R_n = 59.2$ kips

Therefore, $\phi R_n = 59.2$ kips > Ru = 32.6 kips OK

Therefore, transverse stiffeners are not required.

Pick girder W24x55, $b_{fg} = 2.57$ in. > 1.82 in. OK

Check strength for two equal loads loaded symmetrically on W24x55:

$M_U = R_U (a) = 32.6(10) = 326.0$ k-ft

$$Z_R = \frac{M_U}{0.9F_y} = \frac{326(12)}{0.9(50)} = 86.9 in^3$$

W24x55, $Z_x = 134.0$ in^3 > 86.9 in^3 OK

From the proposed Yield Line Equation and Table 5-1, the nominal strength of girder flange (loaded one side) for W24x55 with $b_{fb} = 6.5$ in., $R_n = 40.0$ kips. Assume a value of $\phi = 0.9$.

Therefore, $\phi R_n = 36.0$ kips $> R_U = 32.6$ kips OK

The yield line equation adequately predicts the beam reaction, which was based on a typical office floor and load conditions for an exterior girder.

CHAPTER 6
SUMMARY AND CONCLUSIONS

6.1 SUMMARY

An analytical investigation was carried out to study the behavior of a proposed bottom flange bearing beam-to-girder connection. Five girder specimens were studied and loaded till first yielding in the experimental phase of this research. Results of this testing program are presented in Chapter Two. The analysis portion of this research consists of two sections, i.e., the finite element study as well as the yield line theory. The former is used to validate the experimental results, looking at the behavior of the girders in terms of the first yield load, relative deflection, strains and bending stresses. The latter is used to derive the proposed yield line equation to predict the first yield load. This equation utilizes the material and section properties of both the beam and girder to predict the first yield load. A preliminary design procedure based on the proposed yield line equation looks at several common sections and is presented in Chapter Five.

6.2 CONCLUSIONS AND RECOMMENDATIONS

The results from the finite element study, which includes the W24x68 model with the two bolt holes and the one-sided load to mimic the exterior side of the connection, does not vary significantly with the results when the model is loaded equally on both sides. The next testing phase should include the actual beam-to-girder connection as well as longer spans.

The yield line analysis is sufficient for this study. The predicted failure loads from the proposed model are compared with the experimental results. It is shown that the anticipated loads are conservative. However, the proposed yield line equation can be used to predict the applied load at first yielding. This is because the equation is compared with the applied load where the first yielding occurs, and not the ultimate load of the

particular girder section. Further full-scale testing needs to be done in order to verify the proposed yield line equation and results from the first phase of the research.

The study indicates that the girder flange for all five sections that were considered will be able to carry loads higher than the beam reaction based on a typical office floor bay and the usual loading conditions. However, a detailed probability study is needed in order to determine an accurate resistance factor. Therefore, further full-scale testing is required. If not, the use of the resistance factor for web yielding is an option for the design procedure.

REFERENCES

Manual of Steel Construction: Load and Resistance Factor Design Volume 1 (1998), 2nd ed., American Institute of Steel Construction, Inc., Chicago.

Bakker, M. (1990), "Yield Line Analysis of Post-Collapse Behavior of Thin-walled Steel Members," *Heron*, **35**, 1-50.

Borgsmiller, J. and Murray, T. (1995), *Simplified Method for Design of Moment End-Plate Connections*. Virginia Polytechnic Institute and State University, Blacksburg, VA.

Carter, C. J., Murray, T. and Thornton, W. (1997), "Discussion on 'The Behavior and Load-Carrying Capacity of Unstiffened Seated Beam Connections'," *Engineering Journal*, **34**, 151-156.

Dally J. W. and Riley W. F. (1978), *Experimental Stress Analysis*. 2nd ed., McGraw-Hill, New York.

Gamble, W. L. (2001), Electronic Mail Correspondence dated March 19th 2001, University of Illinois, Urbana-Champaign, IL.

Johansen, K. W. (1962), *Yield Line Theory*. Cement and Concrete Association, London.

Johansen, K. W. (1972), *Yield Line Formulae for Slabs*. 3rd ed., Cement and Concrete Association, London.

Jones, L. L. and Wood R. H. (1967), *Yield-Line Analysis of Slabs*. American Elsevier Publishing, New York.

Liu, T. (1999), "Automatic Computational Method for Yield Line Analysis," *Structural Engineering and Mechanics*, **8**, 311-324.

Mann, A.P. and Morris L. J. (1979), "Limit Design of Extended End-Plate Connections," *Journal of the Structural Division*, ASCE, **105**, 511-526.

Mays, T. W. (2000), *Application of the Finite Element Method to the Seismic Design and Analysis of Large Moment End-Plate Connections*. Ph.D. Dissertation, Virginia Polytechnic Institute and State University, Blacksburg, VA.

Mendelson A. (1968), *Plasticity: Theory and Application*. 1st ed., Macmillan, New York.

Moy, S. (1996), *Plastic Methods for Steel and Concrete Structures*. 2nd ed., Macmillan, Hampshire, United Kingdom.

Moy, S., Troup, S. and Xiao. R. Y. (1998), "Numerical Modeling of Bolted Steel Connections," *Journal of Construction Steel Research*, **46**, 269-276.

Otegui, M. A. (1996*), Simplified Method for Design of Stiffened and Unstiffened Structural Tee Hangers*. Master's Thesis, Virginia Polytechnic Institute and State University, Blacksburg, VA.

Packer, J. A. and Morris L. J. (1977), " A Limit State Design Method for the Tension Region of Bolted Beam-Column Connections," *The Structural Engineer*, **51**, 446-464.

Packer, J. (1989), "A Limit-States Design Method for Welded Tension Connections to I-Section Webs," *Journal of Construction Steel Research*, **12**, 33-53.

Park, R. and Gamble, W. L. (1980), *Reinforced Concrete Slabs*. John Wiley and Sons, New York.

Rasmussen, L. J. and Baker, G. (1998), "A Finite Element Yield Line Model for the Analysis of Reinforced Concrete Plates," *Structural Engineering and Mechanics*, **6**, 395-409.

Ryan, J. C. (1999), *Evaluation of Extended End-Plate Moment Connections under Seismic Loading*. Master Thesis, Virginia Polytechnic Institute and State University, Blacksburg, VA.

Srouji, R. and Murray, T. (1983), "Yield Line Analysis of End-Plate Connections with Bolt Force Predictions," Research Report FSEL/MBMA 83-05, Fears Structural Engineering Laboratory, University of Oklahoma, Norman, OK.

Szilard, R. (1974), *Theory and Analysis of Plates: Classical and Numerical Methods.* Prentice-Hall, New Jersey.

Terry, A. and Easterling, W. S. (2000), *Behavior of Bottom Flange Bearing Beam-to-Girder Connections.* Connections in Steel Structures IV, Roanoke, VA (to appear).

Timoshenko, S. and Woinowsky-Krieger, S. (1959), *Theory of Plates and Shells.* 2nd ed., McGraw-Hill, New York.

Timoshenko, S. (1958), *Strength of Materials Part I: Elementary Theory and Problems.* 2nd ed., R. E. Krieger Publishing, New York.

Thavalingam, A. (1999), "Computer-assisted Generation of Yield Line Patterns for Uniformly Loaded Isotropic Slabs Using an Optimization Strategy," *Engineering Structures*, **21**, 488-496.

APPENDIX A

Proposed Yield Line Equation Derivation

Derivation of Yield Line Equation

Assume a unit deflection at the flange edge:

$$\theta_1 := \frac{1}{b_g} \qquad (1) \qquad\qquad \theta_1 := \frac{h}{b_g - \frac{d}{2}} \qquad (2)$$

Equating (1) and (2):

$$h := 1 - \frac{d}{2 \cdot b_g}$$

$$\theta_x := \frac{1}{b_g} \qquad\qquad \theta_y := \frac{1}{a}$$

$$m_{px} := m_p \cdot \cos\theta \qquad\qquad m_{py} := m_p \cdot \sin\theta$$

$$m_{px} := \frac{m_p \cdot a}{\sqrt{b_g^2 + a^2}} \qquad (3) \qquad\qquad m_{py} := \frac{m_p \cdot b_g}{\sqrt{b_g^2 + a^2}} \qquad (4)$$

Internal work, $W_i := \Sigma m_{px} + m_{py}$

$$W_i := m_p \cdot \left(\frac{1}{b_g}\right) \cdot (b_b) + 2 \cdot m_p \cdot \left(\frac{1}{a}\right) \cdot (b_g) + 2 \cdot m_p \cdot \frac{a}{\sqrt{b_g^2 + a^2}} \cdot \left(\frac{1}{b_g}\right) \cdot \left(\sqrt{b_g^2 + a^2}\right) + 2 \cdot m_p \cdot \frac{b_g}{\sqrt{b_g^2 + a^2}} \cdot \left(\frac{1}{a}\right) \cdot \left(\sqrt{b_g^2 + a^2}\right)$$

Simplify the equation above to obtain:

$$W_i := m_p \cdot \left(\frac{b_b}{b_g}\right) + 4 \cdot m_p \cdot \left(\frac{b_g}{a}\right) + 2 \cdot m_p \cdot \left(\frac{a}{b_g}\right) \qquad (5)$$

External work, $W_e := R \cdot \left(1 - \frac{d}{2 \cdot b_g}\right)$ (6)

where R = Load applied

To find unknown a, set $\frac{dW_i}{da} := 0$

$$\frac{dW_i}{da} := 2 \cdot m_p \cdot \left(\frac{1}{b_g}\right) - 4 \cdot m_p \left(\frac{b_g}{a^2}\right)$$

$$2 \cdot m_p \cdot \left(\frac{1}{b_g} - 2 \cdot \frac{b_g}{a^2}\right) := 0$$

Solving for a: $a := \sqrt{2} \cdot b_g$ (7)

Equating (5) and (6) and knowing $m_p := \frac{F_y \left(t_f^2\right)}{4}$

$$R := F_y \cdot t_f^2 \cdot \frac{\left(\frac{b_b}{4 \cdot b_g} + \frac{2}{\sqrt{2}}\right)}{\left(1 - \frac{d}{2 \cdot b_g}\right)} \qquad (8)$$

APPENDIX B

ANSYS Model Results

ANSYS MODELS

W18x40

Load (kips)	Midspan Edge Deflection (in.)	Midspan Deflection (in.)	Relative Deflection (in.)
0.0	0.000	0.000	0.000
37.3	-0.069	-0.051	-0.018
74.7	-0.138	-0.102	-0.037
130.7	-0.292	-0.197	-0.095
186.7	-0.877	-0.591	-0.285
224.0	-1.867	-1.401	-0.466

W18x50

Load (kips)	Midspan Edge Deflection (in.)	Midspan Deflection (in.)	Relative Deflection (in.)
0.0	0.000	0.000	0.000
37.3	-0.058	-0.026	-0.033
74.7	-0.117	-0.052	-0.065
130.7	-0.226	-0.094	-0.131
177.3	-0.429	-0.150	-0.278
224.0	-0.760	-0.235	-0.525

W21x44

Load (kips)	Midspan Edge Deflection (in.)	Midspan Deflection (in.)	Relative Deflection (in.)
0.0	0.000	0.000	0.000
37.3	-0.069	-0.040	-0.029
74.7	-0.139	-0.079	-0.060
130.7	-0.339	-0.156	-0.183
186.7	-0.790	-0.295	-0.495
203.5	-0.981	-0.368	-0.613
213.7	-1.114	-0.424	-0.690
224.0	-1.258	-0.489	-0.769

W24x55

Load (kips)	Midspan Edge Deflection (in.)	Midspan Deflection (in.)	Relative Deflection (in.)
0.0	0.000	0.000	0.000
37.3	-0.063	-0.028	-0.035
74.7	-0.125	-0.055	-0.070
130.7	-0.247	-0.101	-0.146
186.7	-0.560	-0.173	-0.387
224.0	-0.866	-0.235	-0.631

W24x68

Load (kips)	Midspan Edge Deflection (in.)	Midspan Deflection (in.)	Relative Deflection (in.)
0.0	0.000	0.000	0.000
37.3	-0.071	-0.015	-0.056
74.7	-0.143	-0.030	-0.113
130.7	-0.291	-0.055	-0.236
177.3	-0.615	-0.089	-0.526
198.3	-0.823	-0.109	-0.715
211.2	-0.961	-0.121	-0.840
224.0	-1.098	-0.133	-0.965

W24x68 with Two Bolt Holes

Load (kips)	Midspan Edge Deflection (in.)	Midspan Deflection (in.)	Relative Deflection (in.)
0.0	0.000	0.000	0.000
37.3	-0.070	-0.015	-0.055
74.7	-0.141	-0.030	-0.111
130.7	-0.282	-0.055	-0.227
186.7	-0.660	-0.102	-0.559
224.0	-1.032	-0.142	-0.890

W24x68 with One-Sided Load

Load (kips)	Midspan Edge Deflection (in.)	Midspan Deflection (in.)	Relative Deflection (in.)
0.0	0.000	0.000	0.000
18.7	-0.031	-0.008	-0.024
37.3	-0.063	-0.015	-0.048
65.3	-0.115	-0.026	-0.089
88.7	-0.195	-0.036	-0.159
112.0	-0.363	-0.046	-0.316
147.0	-0.652	-0.060	-0.592

VITA

Wey-Jen Lee was born in Taiping, Malaysia on February 20th 1978. After graduating from high school in 1995, he pursued a Bachelor of Science in Civil Engineering at Purdue University, West Lafayette, Indiana. After graduating in December 1999, he started work on a Master of Science in Civil Engineering at Virginia Polytechnic Institute and State University, Blacksburg, Virginia. In summer 2000, he worked for Bechtel Corporation as an intern. He completed his studies in May 2001. Wey-Jen began working for Bechtel Corporation in Frederick, Maryland in June 2001.